Strong clustering of noninteracting, sliding passive scalars driven by fluctuating surfaces

Apoorva Nagar,[1] Satya N. Majumdar,[2] and Mustansir Barma[1]
[1]*Department of Theoretical Physics, Tata Institute of Fundamental Research, Homi Bhabha Road, Mumbai 400 005, India*
[2]*Laboratoire de Physique Theorique et Modeles Statistiques, Universit'e Paris-Sud, Bâtiment 100, Orsay, France*
(Received 25 October 2005; revised manuscript received 20 April 2006; published 29 August 2006)

We study the clustering of passive, noninteracting particles moving under the influence of a fluctuating field and random noise, in one and two dimensions. The fluctuating field in our case is provided by surfaces governed by the Kardar-Parisi-Zhang (KPZ) and the Edwards-Wilkinson (EW) equations, and the sliding particles follow the local surface slope. As the KPZ equation can be mapped to the noisy Burgers equation, the problem translates to that of passive scalars in a Burgers fluid. Monte Carlo simulations on discrete lattice models reveal very strong clustering of the passive particles for all sorts of dynamics under consideration. The resulting strong clustering state is defined using the scaling properties of the two point density-density correlation function. Our simulations show that the state is robust against changing the ratio of update speeds of the surface and particles. We also solve the related equilibrium problem of a stationary surface and finite noise, well known as the Sinai model for random walkers on a random landscape. For this problem, we obtain analytic results which allow closed form expressions to be found for the quantities of interest. Surprisingly, these results for the equilibrium problem show good agreement with the nonequilibrium KPZ problem.

DOI: 10.1103/PhysRevE.74.021124 PACS number(s): 05.40.−a, 47.40.−x, 02.50.−r, 64.75.+g

I. INTRODUCTION

The coupling of two or more driven diffusive systems can give rise to intricate and interesting behavior, and this class of problems has attracted much recent attention. Models of diverse phenomena, such as growth of binary films [1], motion of stuck and flowing grains in a sandpile [2], sedimentation of colloidal crystals [3], movement of ants along a trail [4], and the flow of passive scalars such as ink or dye in fluids [5,6] involve two interacting fields. In this paper, we concentrate on semiautonomously coupled systems—these are systems in which one field evolves independently and drives the second field; passive scalars are typical examples of such systems. Apart from being driven by the independent field, the passive field is also subject to noise, and the combination of driving and diffusion gives rise to interesting behavior. Our aim in this paper is to understand and characterize the steady state of a passive field of this kind.

The passive scalar problem is of considerable interest in the area of fluid mechanics and has been well studied, see Refs. [5,6] for reviews. Apart from numerical studies, considerable understanding has been gained by analyzing the Kraichnan model [6–8] where the velocity field of a fluid is replaced by a correlated Gaussian velocity field. Typical examples of passive scalars such as dye particles or a temperature field advected by a stirred fluid bring to mind pictures of spreading and mixing caused by the combined effect of fluid advection and diffusion. On the other hand, if the fluid is compressible, or if the inertia of the scalars cannot be neglected, the scalars may cluster rather than spread out [9–15]. It has been argued that there is a phase transition as a function of the compressibility of the fluid—at large compressibilities, the particle trajectories implode, while they explode in the incompressible or slightly compressible case [16]. It is the highly compressible case which is of interest in this paper.

Specifically, we study and characterize the steady state properties of passive, noninteracting particles sliding on a fluctuating surface and subject to noise [17,18]. The surface is the autonomously evolving field and the particles slide downwards along the local slope. We consider surfaces evolving according to the Kardar-Parisi-Zhang (KPZ) and the Edwards-Wilkinson (EW) equations. The KPZ equation can be mapped to the well-known Burgers equation with noise, which describes a compressible fluid. Thus the problem of passive particles sliding on a fluctuating surface maps to the problem of passive scalars in a compressible fluid. The nonlinear term in the KPZ equation breaks the up-down symmetry, bringing in the possibility of two kinds of dynamics—particles moving in the direction of average surface motion (particles moving with the flow, advection in fluid language) and particles moving against it (antiadvection). By contrast, the EW model has an up-down symmetry, and hence there is no distinction between advection and antiadvection in this case. We study all three kinds of dynamics mentioned above—KPZ advection, KPZ antiadvection, and EW, in one and two dimensions. Drossel and Kardar [17] were the first to study the steady state properties for the KPZ advection and antiadvection dynamics in one dimension. Using Monte Carlo simulations of a solid on solid model and analyzing the number of particles in a given bin as a function of bin size, they showed that there is clustering of particles. However, their analysis does not involve the scaling with system size, which as we will see below, is one of the most important characteristics of the system. We find that the two point density-density correlation function is a scaling function of r and L (r is the separation and L is the system size) and that the scaling function diverges at small r/L. The divergence indicates formation of large clusters while the scaling of r with L implies that the clusters are typically separated from each other by a distance that scales with the system size. A brief account of some of our results has appeared in Ref. [18].

Scaling of the density-density correlation function with system size has also been observed in the related problem of particles with a hard core interaction, sliding under gravity

on a KPZ surface [19–21] or advected by director flucuations in a two-dimensional nematic [22]. However, the correlation function in this case has a cusp singularity as $r/L \to 0$, in contrast to the divergence that we find for noninteracting particles. Thus, while clustering and strong fluctuations are seen in both, the nature of the steady states is different in the two cases. In our case, clustering of the noninteracting particles causes a vanishing fraction of sites to be occupied, whereas hard core interactions force the occupancy of a finite fraction. In the latter case, there are analogies to customary phase ordered states, with the important difference that there are strong fluctuations in the thermodynamic limit, leading to the appellation fluctuation dominated phase ordering (FDPO) states. The terminology strong clustering states (SCS) is reserved for the sort of nonequilibrium states that are found with noninteracting particles—a key feature being the divergent scaling function describing the two point correlation function. The feature of strong fluctuations is also present in the SCS. In the case of KPZ advection, various observables have broad distributions in the thermodynamic limit implying that they are non-self-averaging.

In the problem defined above, there are two time scales involved, one associated with the surface evolution and the other with particle motion. We define ω as the ratio of the surface to the particle update rates. We study the variations in the steady state characteristics of the system when ω is varied. We see that the steady state is always an SCS for finite values of ω. The limit of $\omega \to 0$ is of special importance. There is a slight subtlety here as the limit $\omega \to 0$ does not commute with the thermodynamic limit $L \to \infty$. If we consider taking $\omega \to 0$ first and then approach large system size ($L \to \infty$), we obtain a state in which the surface is stationary and the particles move on it under the effect of noise. In this limit of a stationary surface, we obtain an equilibrium problem. This is the well-known Sinai model which describes random walkers in a random medium. We will discuss this limit further below. Now consider taking the large system size limit first and then approach $\omega=0$; this describes a system in which particles move extremely fast compared to the evolution of the local landscape. This leads to the particles settling quickly into local valleys, and staying there until a new valley evolves. We thus see a nonequilibrium SCS state here, but with the feature that the probability of finding a large cluster of particles on a single site is strongly enhanced. The opposite limit is the $\omega \to \infty$ limit where the surface moves much faster than the particles. Because of this very fast movement, the particles do not get time to "feel" the valleys and they behave as nearly free random walkers.

The equilibrium limit ($\omega \to 0$ followed by $L \to \infty$), in one dimension, coincides with the Sinai model describing random walkers in a random medium [23]. This problem can be analyzed analytically by mapping it to a supersymmetric quantum mechanics problem [24] and we are able to obtain closed form answers for the two quantities of interest—the two point correlation function $G(r,L)$ and the probability distribution function of finding n particles on a site $P(n,L)$. Surprisingly, we find that not only is the equilibrium state an SCS, but the functional forms obtained in this limit agree very well with our results on KPZ advection. The only free parameter in this equilibrium problem is the temperature and we choose it to fit our numerical data for the nonequilibrium system. Interestingly, the effective temperature seems to depend on the quantity under study.

Apart from the static quantities studied above, one can also study the dynamic properties of the system. Bohr and Pikovsky [25] and Chin [26] have studied dynamic quantities for a model similar to our KPZ advection (one dimension), with the difference that they do not consider noise acting on particles. In the absence of noise, all the particles coalesce and ultimately form a single cluster in steady state, very different from the strongly fluctuating, distributed particle state under study here. References [25] and [26] study the process of coalescence in time. Further, they find that the rms displacement for a given particle increases in time t as $t^{1/z}$, where z is equal to the dynamic exponent of the surface, indicating that the particles have a tendency to follow the valleys of the surface. Drossel and Kardar [17] have studied the rms displacement in the same problem in the presence of noise and observe the same behavior. We confirm this result in our simulations and observe that the variation of ω does not change the result. Gopalakrishnan [27] has studied the variation of rms displacement of passive sliders on a one-dimensional EW surface, and the possibility was raised that there are two different exponents characterizing this quantity for $\omega \leqslant 1$ and for $\omega > 1$. We give numerical evidence that the apparent change in exponent with change in ω is due to a crossover effect and that there is a single exponent which describes the rms displacement.

The arrangement of this paper is as follows. In Sec. II, we will describe the problem in terms of continuum equations and then describe discrete lattice models, in one dimension, which mimic these equations at large length and time scales. We have used these models to study the problem via Monte Carlo simulations. Section III describes results of our numerical simulations for surfaces in one dimension. We start with detailed results for the KPZ advection case. We will then describe our results for the KPZ antiadvection and EW cases. Section IV describes our analytic results for the equilibrium Sinai limit of a static surface and the surprising connection with results for the nonequilibrium problem of KPZ/Burgers advection. Section V describes the lattice model and our results for the problem in two dimensions with the same three cases as above, namely KPZ advection, KPZ antiadvection, and EW dynamics.

II. DESCRIPTION OF THE PROBLEM

We consider surfaces that evolve according to the KPZ and EW equations. The KPZ equation [28] is

$$\frac{\partial h}{\partial t} = \nu \nabla^2 h + \frac{\lambda}{2}(\nabla h)^2 + \zeta_h(\vec{x},t). \tag{1}$$

Here h is the height field and ζ_h is a Gaussian white noise satisfying $\langle \zeta_h(\vec{x},t)\zeta_h(\vec{x}',t')\rangle = 2D_h \delta^d(\vec{x}-\vec{x}')\delta(t-t')$. The passive particles sliding on the surface satisfy

$$\frac{d\vec{x}_m}{dt} = -a\ \nabla h|_{\vec{x}_m} + \zeta_m(t), \tag{2}$$

where $\vec{x}_m$ is the position of the mth particle. The white noise $\zeta_m(t)$ represents the randomizing effect of temperature, and satisfies $\langle \zeta_m(t)\zeta_m(t')\rangle = 2\kappa\delta(t-t')$. The transformation $\vec{v} = -\nabla h$ maps Eq. (1) (with $\lambda = 1$) to the Burgers equation [Eq. (3) below] which describes a compressible fluid with local velocity $\vec{v}$. As explained later, the ratio $a/\lambda > 0$ corresponds to particles moving with the flow—the KPZ advection case. The case $a/\lambda < 0$ corresponds to KPZ antiadvection which corresponds to particles moving against the flow in the fluid picture. The Burgers equation with noise

$$\frac{\partial \vec{v}}{\partial t} + \lambda(\vec{v}\cdot\nabla\vec{v}) = \nu\nabla^2\vec{v} + \nabla\zeta_h(\vec{x},t) \tag{3}$$

describes a compressible fluid because it does not have the pressure term, which is present in the Navier-Stokes equation. The transformed Eq. (2) ($\vec{v} = -\nabla h$) describes passive scalar particles advected by the Burgers fluid.

The other interface dynamics we consider is the Edwards-Wilkinson (EW) model, where the height field evolves via the linear equation,

$$\frac{\partial h}{\partial t} = \nu\nabla^2 h + \zeta_h(\vec{x},t). \tag{4}$$

The above equation does not have the up-down symmetry-breaking nonlinear term $(\nabla h)^2$, so the interface has no average up or down movement and thus no advection or antiadvection subcases. The passive sliders again follow Eq. (2).

In this paper, we will describe our results on the above coupled equations Eqs. (1) and (2) and Eqs. (4) and (2) in one and two dimensions. Rather than solving these equations numerically, we perform Monte Carlo simulations on lattice models which mimic the behavior of the equations at large length and time scales. We describe these lattice models below.

Lattice models for Monte Carlo simulations, one dimension

The model consists of a flexible, one-dimensional lattice in which particles reside on sites, while the links or bonds between successive lattice sites are also dynamical variables which denote local slopes of the surface. The total number of sites is L and the total number of particles N is taken to be equal to L in our simulations. Each link takes either of the values +1 (upward slope $\rightarrow/$) or −1 (downward slope $\rightarrow\backslash$). The rules for surface evolution are:

KPZ advection: Choose a site at random, and if it is on a local hill ($\wedge$), change the local hill to a local valley ($\vee$) (Fig. 1, extreme left). After every N_s surface moves, we perform N_p particle updates according to the following rule: we choose a particle at random and move it one step downward with probability $(1+K)/2$ or upward with probability $(1-K)/2$. The parameter K ranges from 1 (particles totally following the surface slope) to 0 (particles moving independently of the surface). In our simulations, we update the surface and particles at independent sites, reflecting the independence of the noises $\zeta_h(x,t)$ and $\zeta_m(t)$ [29]. The ratio $\omega \equiv N_s/N_p$ controls the relative time scales of the surface evolution and particle movement. In particular, the limit $\omega \rightarrow 0$, with L held fixed, corresponds to the adiabatic limit of the problem where particles move on a static surface and the steady state is the thermal equilibrium state.

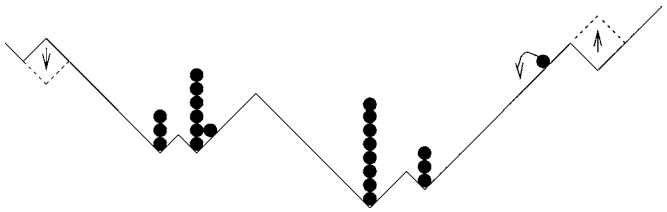

FIG. 1. Schematic diagram of the surface and noninteracting particles sliding on top of it. Arrows show possible surface and particle moves.

KPZ antiadvection: Choose a site at random, and if it is on a local valley ($\vee$), change the local valley to a local hill ($\wedge$) (Fig. 1, extreme right). The particle moves are the same as in advection.

EW: We allow for both the motions—local hill to local valley, and local valley to local hill, with equal probabilities. The particle moves are again the same as in advection and antiadvection above.

To see how the lattice model described above describes a KPZ surface, consider the mapping of the above model to the well-known asymmetric simple exclusion process (ASEP): consider an up slope to be a particle on a lattice and a down slope to be an empty space (hole). The flipping of a hill to a valley then corresponds to the motion of a particle (exchange of particle and hole). A coarse grained description of the ASEP leads to the KPZ equation [30]. The continuum description of the ASEP, obtained by coarse graining over regions which are large enough to contain many sites, involves the density of particles $\rho(x)$ and the local current $J(x)$. These are connected through the continuity equation

$$\frac{\partial\rho}{\partial t} + \frac{\partial J}{\partial x} = 0. \tag{5}$$

The local current can be written as

$$J(x) = -\nu\frac{\partial\rho}{\partial x} + j(\rho) + \eta, \tag{6}$$

where ν is the particle diffusion constant, η is a Gaussian noise variable, and $j(\rho)$ is the systematic contribution to the current associated with the local density ρ. Using the expression for the bulk ASEP with density ρ for j, we have

$$j(\rho) = (p-q)\rho(1-\rho), \tag{7}$$

where p and q are the particle hopping probabilities to the right and left, respectively, with our one-step model corresponding to $p=1$ and $q=0$.

Since we identify the presence (absence) of a particle in the lattice model with an up (down) slope, we may write

$$\rho = \frac{1}{2}\left(1 + \frac{\partial h}{\partial x}\right). \tag{8}$$

Using Eqs. (6)–(8) in Eq. (5) leads to

$$\frac{\partial h}{\partial t} = -\frac{1}{2}(p-q) + \nu\frac{\partial^2 h}{\partial x^2} + \frac{1}{2}(p-q)\left(\frac{\partial h}{\partial x}\right)^2 - 2\eta \qquad (9)$$

which is the KPZ equation [Eq. (1)] in one dimension with an additional constant term, and $\lambda=(p-q)$ and $\zeta_h=-2\eta$. Note that the signs of the constant term and λ are opposite. Thus a downward moving surface (corresponding to $p>q$) has positive λ. The constant term can be eliminated by the boost $h\to h-\frac{1}{2}(p-q)t$, but its sign is important in determining the overall direction of motion of the surface. The case $(a/\lambda)>0$ which is of interest to us thus corresponds to the lattice model in which particles move in the same direction as the overall surface motion.

The parameters ω and K defined in the lattice model are connected to the continuum equations as follows. In the limit of a stationary surface, we achieve equilibrium and the particles settle into a Boltzmann state with particle density $\sim e^{-\beta h(x)}$, here $h(x)$ is the surface height profile and β is the inverse temperature. β is related to K by $\beta=\ln\left(\frac{1+K}{1-K}\right)$ and to the parameters a and κ in Eq. (2) by $\beta=a/\kappa$. Thus

$$K = \frac{e^{a/\kappa}-1}{e^{a/\kappa}+1}. \qquad (10)$$

The parameter ω cannot be written simply in terms of the parameters in the continuum equations, because it modifies Eqs. (1) and (4) as we now show. ω is the ratio of the update speeds or equivalently the time between successive updates of the particles Δt_p and surface Δt_s. The noises $\zeta_h(\vec{x},t)$ and $\zeta_m(t)$ in Eqs. (1) and (2) can be written as $\sqrt{\frac{D_h}{\Delta t_s}}\tilde{\zeta}_h(\vec{x},t)$ and $\sqrt{\frac{\kappa}{\Delta t_p}}\tilde{\zeta}_m(t)$, respectively. Here $\tilde{\zeta}_h(\vec{x},t)$ is noise of $O(1)$, uncorrelated in time, white in space while $\tilde{\zeta}_m(t)$ is uncorrelated noise of $O(1)$. The factors of $\sqrt{\frac{1}{\Delta t}}$ in the terms indicate that the strength of the noise depends on how frequently noise impulses are given to the particles; the square root arises from the random nature of these impulses. Thus the change in height Δh in time Δt_s and the distance traveled $\Delta\vec{x}_m$ in time Δt_p are, respectively,

$$\Delta h = \Delta t_s\left[\nu\nabla^2 h + \frac{\lambda}{2}(\nabla h)^2\right] + \sqrt{\Delta t_s D_h}\tilde{\zeta}_h(\vec{x},t), \qquad (11)$$

$$\Delta\vec{x}_m = \Delta t_p[-a\ \nabla h|_{\vec{x}_m}] + \sqrt{\Delta t_p\kappa}\tilde{\zeta}(t). \qquad (12)$$

We now identify Δt_s and Δt_p with the Monte Carlo time step δt as $\Delta t_s=N_s\delta t$ and $\Delta t_p=N_p\delta t$. We can thus replace Δt_s by $\omega\Delta t_p$ and take it to be the natural continuous time. We thus get

$$\frac{\partial h}{\partial t} = \omega\left[\nu\nabla^2 h + \frac{\lambda}{2}(\nabla h)^2\right] + \sqrt{\omega}\zeta_h(\vec{x},t), \qquad (13)$$

$$\frac{d\vec{x}_m}{dt} = -a\ \nabla h|_{\vec{x}_m} + \zeta_m(t). \qquad (14)$$

We can see that the ω dependence in the above equation cannot be removed by a simple rescaling of the parameters of the equation. Equation (1) is recovered as a special case of Eq. (13) on setting $\omega=1$. The same analysis can be carried through for the EW equation by dropping the nonlinear term in the equations above.

III. NUMERICAL RESULTS, ONE DIMENSION

A. KPZ advection

We will first describe our results on the KPZ advection case in one dimension, a brief description of which has already been given in Ref. [18]. We start with the simplest case $\omega=K=1$; surface updates are attempted as frequently as particle updates, and both particles and surface always move only downwards. In our simulations, we work with $N=L$, where N is the total number of particles and there are L sites in the lattice. For a given L, we first evolve the system into its steady state and then sample data every 1000 Monte Carlo time steps to reduce correlation between samples. We average over a total of 30,000 samples.

1. Two point density-density correlation function

The two point density-density correlation function is defined as $G(r,L)=\langle n_i n_{i+r}\rangle_L$, where n_i is the number of particles at site i. Figure 2 shows the scaling collapse of numerical data for various system sizes L which strongly suggests that for $r>0$, the scaling form

$$G(r,L) \sim \frac{1}{L^\theta}Y\left(\frac{r}{L}\right) \qquad (15)$$

is valid with $\theta\simeq 1/2$. The scaling function $Y(y)$ has a power law divergence $Y(y)\sim y^{-\nu}$ as $y\to 0$, with ν close to 3/2 (see Table I). The data for $r=0$ points to $G(0,L)\sim L$.

The result in Eq. (15) is in agreement with an exact result of Derrida *et al.* [31] for a slightly different model. As we have seen in the previous section, the single step model which we use for Monte Carlo simulations can be mapped on to an asymmetric simple exclusion process (ASEP). The particles/holes in the ASEP map to the up/down slopes in our model and the flipping of a hill to a valley is equivalent to swapping a particle with a hole. In Ref. [31], apart from particles and holes, a third species, namely second-class particles, is introduced which acts as holes for the particles and particles for the holes. When translated to the surface language, these second class particles behave like the sliders in our model, with the difference that they are not passive: there is no surface evolution at a site where second-class particles reside. The effect of nonpassivity is relatively unimportant for KPZ advectionlike dynamics of the surface, as particles mostly reside on stable local valleys while surface evolution occurs at local hilltops. Moreover, if the number of second class particles is small, the probability of the rare event where they affect the dynamics of local hills goes down even further. With only two such particles in the full lattice, the probability $p(r)$ that they are at a distance r, is proportional to the two point correlation function $G(r,L)$. The exact result [31] $p(r)\sim\frac{1}{r^{3/2}}$ matches very well with our prediction for the same quantity, $p(r)=\frac{L}{N^2}G(r,L)\sim\frac{1}{r^{3/2}}$.

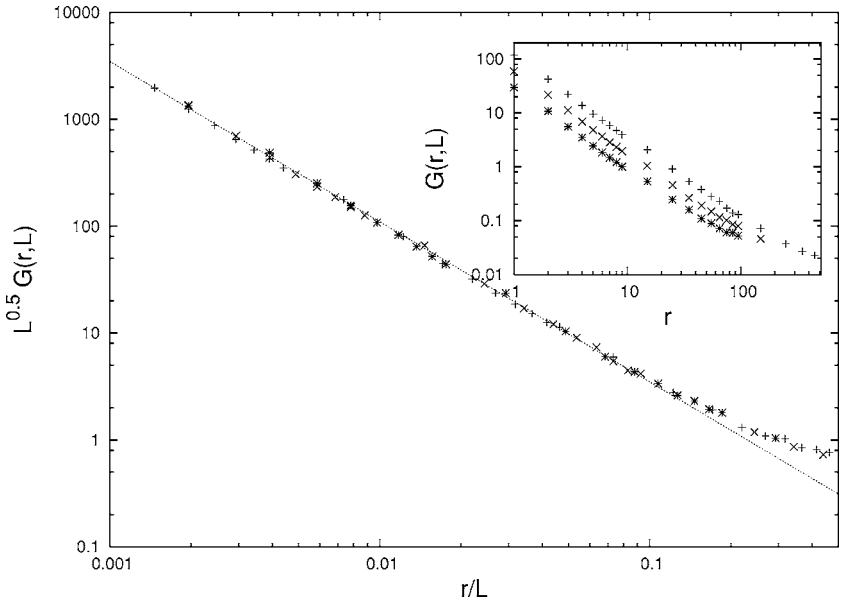

FIG. 2. The inset shows $G(r,L)$ vs r for different values of L. The main plot shows the scaling collapse when r is scaled with L and $G(r,L)$ with $1/L^{0.5}$. The dashed, straight line shows a power law with exponent −1.5. The lattice sizes are $L=512$ (∗), 1024 (×), and 2048 (+).

The result for $G(r,L)$ also allows us to calculate the quantity $N(l,L)$ first defined in Ref. [17]; the lattice is divided into L/l bins of size l and we ask for the number $N(l,L)$ of particles in the same bin as a randomly chosen particle. $N(l,L)$ is a good measure of clustering—if $N(l,L)$ rises linearly with l, one concludes that the particles are fairly spread out, while if $N(l,L)$ saturates or shows a decreasing slope, one concludes that particles are clustered. $N(l,L)$ is related to the two point correlation function through $N(l,L)=\int_0^l G(r,L)dr$, using which we obtain $N(l,L)\sim c_1 L(1-c_2 l^{-\nu+1})$. This form fits the numerical result for N better (Fig. 3) than the l-independent form of Ref. [17].

2. Probability density of occupancy

Another quantity of primary interest is the fraction of sites $P(n,L)$ that are occupied by n particles, which is the same as the probability that any given site has an occupancy n. If $\mathcal{N}_n$ is the number of sites which have an occupancy of n, we define $P(n,L)$ as $P(n,L)\equiv\langle\mathcal{N}_n/L\rangle$, where the brackets indicate an average over configurations. For $n>0$, this quantity shows a scaling with the total number of particles, which in turn is proportional to the system size L. We have (see Fig. 4)

TABLE I. The values of the exponents in one dimension for the three kinds of dynamics under consideration—KPZ advection, KPZ antiadvection, and EW. The first row shows the values of exponents for the equilibrium Sinai limit of a stationary surface.

	δ	ν	γ
Equilibrium Sinai limit	1	3/2	1 with log corrections
KPZ advection	1±0.07	1.48±0.04	1.15±0.02 or 1 with log corrections
KPZ antiadvection	0.33±0.09	0.31±0.02	1.70±0.02
EW	0.68±0.08	0.67±0.02	1.49±0.04

$$P(n,L)\sim\frac{1}{L^{2\delta}}f\left(\frac{n}{L^{\delta}}\right), \tag{16}$$

with $\delta\simeq 1$ (Table I). The scaling function $f(y)$ seems to fit well to a power law $y^{-\gamma}$ with $\gamma\simeq 1.15$ (Fig. 4, Table I), though as we shall see in Sec. IV, the small y behavior may follow $y^{-1}\ln y$. We can use the scaling form in the above equation to calculate $G(0,L)$, $\langle n^2\rangle\equiv G(0,L)=\int_0^L n^2 P(n,L)dn \sim L^{\delta}=L$, which, as we have seen above, is borne out independently by the numerics. Numerical data for $P(0,L)$ [which is not a part of the scaling function in Eq. (16)] shows that the number of occupied sites $N_{occ}\equiv[1-P(0,L)]L$ varies as L^{ϕ} with $\phi\simeq 0.23$, though the effective exponent seems to decrease systematically with increasing system size L.

3. Results on dynamics

The root-mean-square (rms) displacement $R(t)=\langle[x(t)-x(0)]^2\rangle^{1/2}$ of a tagged particle has been studied earlier [17,26]. $R(t)$ is found to obey the scaling form

$$R(t)=L^{\chi}h\left(\frac{t}{L^{z}}\right), \tag{17}$$

where $h(y)\sim y^{1/z}$, with $z=3/2$ for small y. The requirement that $R(t)$ has to be independent of L in the limit $L\to\infty$ leads to $\chi=1$. The value of z above is the same as the dynamic exponent of the KPZ surface. The dynamic exponent z_s of a surface carries information about the time scale of evolution of valleys and hills; the landscape evolves under surface evolution and valleys/hills of breadth L' are typically replaced by hills/valleys in time of order L'^{z_s}. Thus the observation $z=z_s$ suggests that the particles follow the valley movement.

We have also evaluated the autocorrelation function $\tilde{G}(t,L)\equiv\langle n_i(0)n_i(t)\rangle_L$ and find that it scales with the system size as

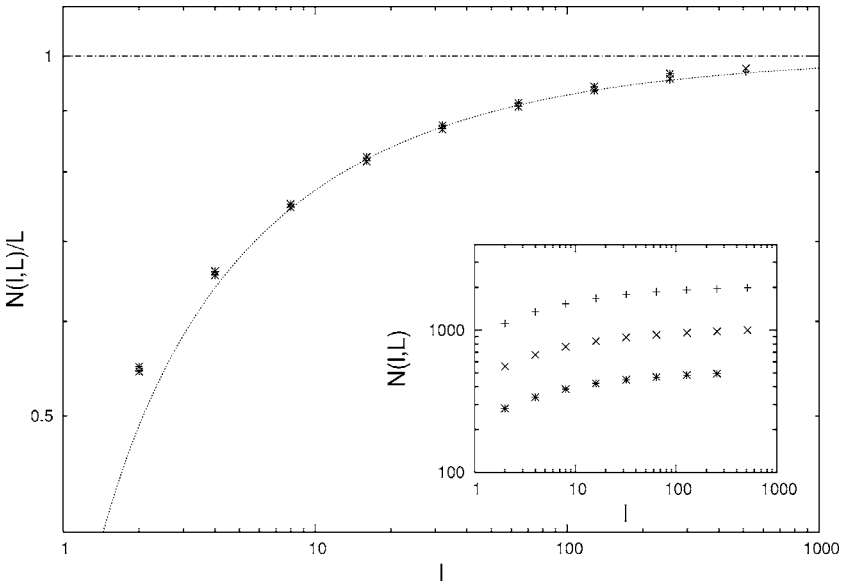

FIG. 3. The inset shows $N(l,L)$ vs bin size l for different system sizes (L). The main plot shows $N(l,L)$ scaled with L vs bin size l. The curve shows $c_1L(1-c_2l^{-\nu+1})$ with $c_1=1$ and $c_2=0.72$. The straight line shows $N(l,L)=L$, the form predicted in Ref. [17]. The lattice sizes are $L=512$ (∗), 1024 (×), and 2048 (+).

$$\tilde{G}(t,L) \sim \tilde{Y}\left(\frac{t}{L^z}\right). \tag{18}$$

Again, $z=z_s=3/2$, reaffirming our conclusion that particles tend to follow valleys. The scaling function shows a power law behavior $\tilde{Y}(\tilde{y}) \sim \tilde{y}^{-\psi}$ with $\psi \simeq 2/3$ as $\tilde{y} \to 0$.

4. Relations between the exponents

The exponents defined in the above sections can be connected to each other by simple relations using scaling analysis. For instance, δ, ν, and θ are related by

$$\delta = \nu - \theta. \tag{19}$$

This can be proved by substituting the scaling form of Eq. (15) and $G(0,L)=\int_0^L n^2 P(n,L)dn \sim L^\delta$ in the equation $\int_0^L G(r,L)dr=L$; the last equation can be obtained by using the definition of $G(r,L)$ and using $N=L$. We can also relate ϕ, δ, and γ by

$$\phi = \delta(\gamma - 2) + 1, \tag{20}$$

which can be derived using the normalization condition $\int_0^L P(n,L)dr=1$ and then substituting for $P(0,L)$ and the scaling form of Eq. (16). Our results from simulations are consistent with these relations.

5. Fluctuations and non-self-averaging

It is known for the problem of hard core particles sliding on fluctuating surfaces [19–21] that there is a clustering of particles and the clusters are highly dynamic in nature—they are continuously breaking into smaller clusters and then recombining to form larger clusters. In fact these fluctuations are so strong that they do not damp down in the thermodynamic limit, leading to the nomenclature fluctuation dominated phase ordering (FDPO). Our system also shows strong fluctuations in the steady state, which we characterize using the fraction of sites $\mathcal{N}_n/L$ with occupancy n. This fraction fluctuates from sample to sample and has a very broad distribution. Its mean is given by $P(n,L)=\langle \mathcal{N}_n \rangle / L$ and its variance by

$$\sigma^2 \equiv \left\langle \left(\frac{\mathcal{N}_n}{L}\right)^2 \right\rangle - \left\langle \frac{\mathcal{N}_n}{L} \right\rangle^2. \tag{21}$$

We found that if n is held fixed and we take the limit $L \to \infty$, the ratio $\sigma / \langle \mathcal{N}_n/L \rangle$ approaches a constant. This is to be contrasted with a normal, self-averaging system where this ratio vanishes in the limit $L \to \infty$.

6. The strong clustering state (SCS)

The following picture of the steady state emerges from our results. The scaling of the probability distribution $P(n,L)$ as n/L and the vanishing of the probability of finding an occupied site ($\equiv N_{occ}/L$) suggest that a large number of particles (often of the order of system size) aggregate on a few sites. The scaling of the two-point density-density correlation function with L implies that the particles are distributed over distances of the order of L, while the divergence of the scaling function indicates clustering of large-mass aggregates. Thus the evidence points to a state where the particles form a few, dense clusters composed of a small number of large mass aggregates and these clusters are separated on the scale of system size. We choose to call this state as the strong clustering state (SCS). The divergence at the origin of the two-point density-density correlation function as a function of the separation scaled by the system size is its hallmark. The information we get from results on dynamics is that the particles have a tendency to follow the surface. This is brought out by the fact that the scaling exponent describing the rms displacement comes out to be equal to the dynamic exponent of the KPZ surface.

7. Variation of ω

To see how the system behaves when we change the relative speeds of the surface and particle evolution, we vary the parameter $\omega \equiv N_s/N_p$ (N_s and N_p being, respectively, the

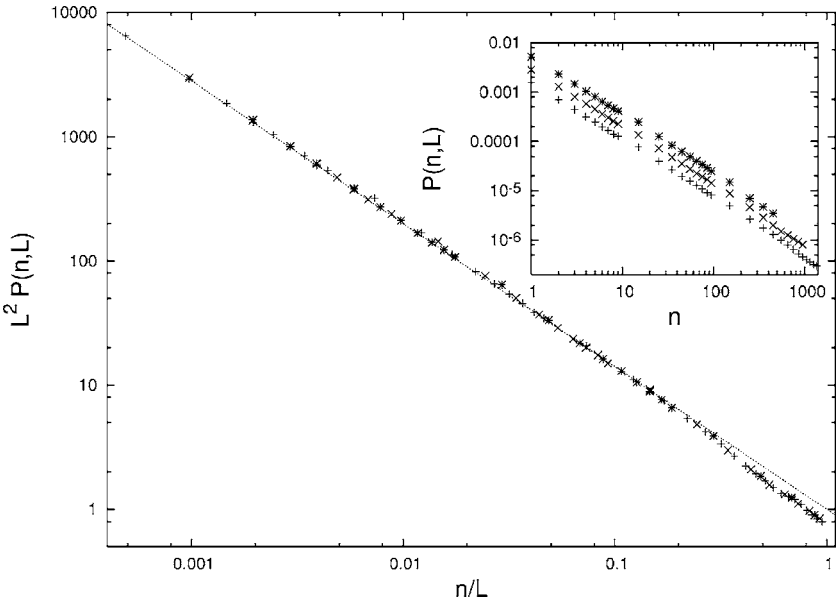

FIG. 4. The inset shows $P(n,L)$ vs n for different values of L. The main plot shows $L^2P(n,L)$ vs n/L. The straight line shows a power law with exponent −1.15. The lattice sizes are $L=512$ (∗), 1024 (×), and 2048 (+).

number of successive surface and particle update attempts) in the range $1/4 \leqslant \omega \leqslant 4$. When $0<\omega<1$ (particles faster than the surface), we regain the scaling form of Eq. (15) for the two point correlation function. The scaling function also diverges with the same exponent. While the probability distribution for occupancy $P(n,L)$ shows similar scaling with system size as Eq. (16), the scaling function $f(y)$ shows a new feature—it develops a peak at large n (Fig. 5). This peak at large n indicates that the probability of finding nearly all the particles at a single site is substantial. A heuristic argument for the appearance of this peak is now given. Consider a configuration in which a large number of particles (nearly equal to the total number of particles) reside in a local valley. When this valley is replaced by another one nearby under surface dynamics, all the particles tend to move to the new one. If the number of particle updates is greater than surface updates, there is a substantial probability that all the particles are able to move to the new valley before it is itself replaced by another one. Thus there is a significant probability of the initial cluster surviving intact for a fair amount of time. Numerically, we also find that

$$\frac{P(n=N,L)}{P(n=N-1,L)} = \frac{1}{\omega}. \tag{22}$$

As mentioned in the Introduction, the case of $\omega=0$ (with the limit $L\to\infty$ taken later) is special. In this case, the problem reduces to an equilibrium problem and can be analytically approached. We will describe the calculations in a separate section below but point out the main result here—the strong clustering state survives for $\omega=0$ and the results (scaling exponents, functional forms of the scaling functions) match very well with our nonequilibrium numerical results for $\omega=1$.

For $\omega>1$, the particles settle down slowly in valleys and $\tau_{surf} \gg \tau_{part}$ where τ_{surf} and τ_{part} are, respectively, the times

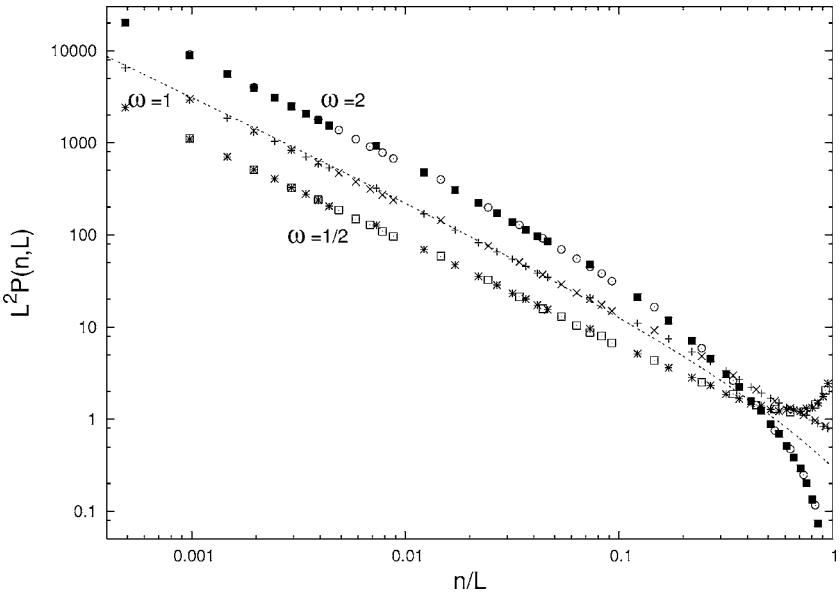

FIG. 5. Scaled probability distribution $P(n,L)$ for $\omega=1/2,1,2$ ($K=1$). The line is a plot of Eq. (72) with $\beta=2.3$. The lattice sizes are $L=1024$ (○, ×, □), and 2048 (■, +, ∗).

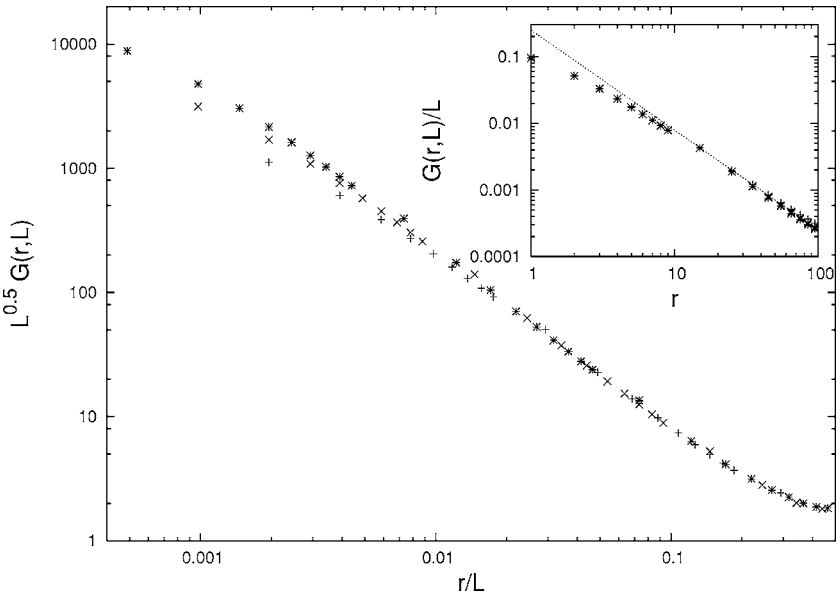

FIG. 6. The main plot shows the scaled two point correlation function for $\omega=2$, $(K=1)$. We see deviation from scaling at small r. The inset shows a plot of $G(r,L)/L$ vs r. The straight line shows a power law with exponent -1.5. The lattice sizes are $L=512$ $(+)$, 1024 $(\times)$, and 2048 $(*)$.

between successive surface and particle updates. Though $\tau_{surf} \gg \tau_{part}$; for large enough L, the survival time of the largest valley $\sim \tau_{surf} L^z$ is always greater than the particle sliding time $\sim \tau_{part} L$. Thus we expect that particles will lag behind the freshly formed valleys of small sizes but would manage to cluster in the larger and deeper valleys, which survive long enough. We thus expect a clustering of particles and scaling to hold beyond a crossover length scale $r_c(\omega)$. We can estimate the crossover length by equating the time scales of surface and particle rearrangements—$\tau_{surf} r_c^z(\omega) \sim \tau_{part} r_c(\omega)$, which yields $r_c(\omega) \sim \omega^{1/(z-1)}$. Using $z=3/2$, we have $r_c \sim \omega^2$. Numerical simulation results are shown in Fig. 6 which shows that the data deviates from scaling and power law behavior at small r, due to a crossover effect. The data suggests that

$$G(r,L) \sim \frac{1}{L^\theta} Y\left(\frac{r}{L}\right) g\left(\frac{r}{r_c(\omega)}\right). \tag{23}$$

As we can see from Fig. 6 (main graph), the curve flattens out at small values of r, so for $y<1$ $[r<r_c(\omega)]$, the function $g(y)$ in the equation above should follow $g(y) \sim y^{1.5}$ while it should go to a constant for $y>1$. We can determine $r_c(\omega)$ from $G(r,L)$ by separating out the r dependent part; if we scale $G(r,L)$ by L, we obtain the quantity $\frac{1}{r^{1.5}} g\left(\frac{r}{r_c(\omega}\right)$. We can now determine $r_c(\omega)$ as the value or r where the scaled data starts deviating from the power law behavior $r^{-1.5}$. From Fig. 6 (inset) $r_c(\omega=2) \simeq 10$. A similar exercise for $\omega=3$ leads to $r_c(\omega=3) \simeq 20$. A clean determination of $r_c(\omega)$ for $\omega>3$ requires data for very large values of system size, beyond the scope of our computational capabilities.

The probability distribution $P(n,L)$ continues to show the same scaling form [Eq. (16)] for $\omega>1$, but the scaling function $f(y)$ in this case dips at large values of y (Fig. 5) in contrast to the peak seen for $\omega<1$. The exponent z describing the rms displacement of particles remains unchanged under a change in ω, again indicating that particles follow the movement of valleys on the large scale.

In the limit $\omega \to \infty$, the surface movement is much faster than the particle response time. The valleys evolve quickly and disappear before the particles can cluster in them, thus the particles essentially move like random walkers or free particles on a planar landscape. Figure 7 depicts the change in the steady state with change in ω, including the special limit $\omega \to 0$.

B. KPZ antiadvection

Let us now consider the KPZ antiadvection case. As described in the Introduction, in this case the particles tend to move in the opposite direction of the surface motion (against the flow in the fluid picture). If we consider the Monte Carlo update rules, we see that while particles try to cluster in the local valleys, the valleys being unstable themselves, tend to reduce the clustering. The question then arises: does the SCS survive in this case? The answer to this question, as we will see below, is yes. The global or largest valleys survive for a long enough time for the particles to cluster strongly enough. However, the exponents are different from the advection case and indicate less clustering—this is a result of the local valleys being unstable.

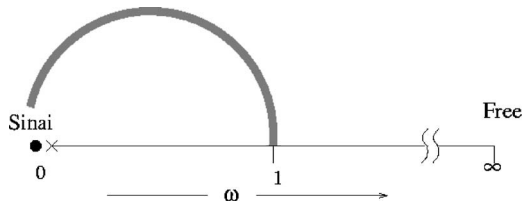

FIG. 7. KPZ advection: Change in state with change in ω. The black circle depicts the Sinai equilibrium limit ($\omega \to 0$ followed by $L \to \infty$). The cross depicts the nonequilibrium SCS with particles moving much faster than the surface ($L \to \infty$ followed by $\omega \to 0$), leading to strong clustering. The gray arc indicates the correspondence between the results in the equilibrium Sinai limit and the nonequilibrium SCS at $\omega=1$. $\omega \to \infty$ is the free particle limit.

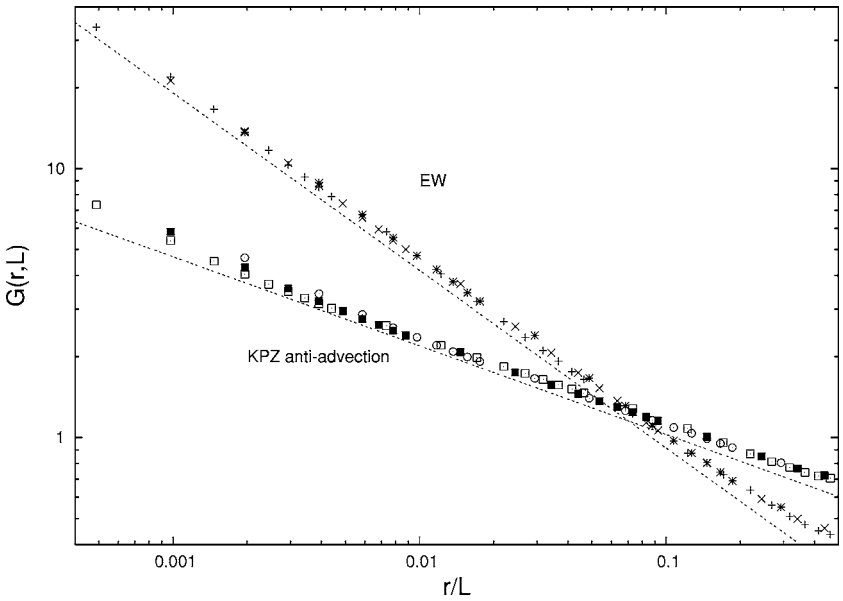

FIG. 8. The figure shows the collapsed data for various values of L when $G(r,L)$ is plotted against r/L. The dotted lines correspond to power laws $Y(y) \sim y^{-\nu}$ with $\nu=2/3$ for the EW data and $\nu=1/3$ for the KPZ antiadvection data. The lattice sizes for both plots are $L=512$ (∗, ○), 1024 (×, ■), and 2048 (+, □).

The two-point correlation in this case has the same form as in Eq. (15) above with $\theta=0$ (Fig 8). We again have a power law divergence with $\nu \simeq 1/3$ (Table I). We also see that $G(0,L) \sim L^{1/3}$. The probability density of occupancy $P(n,L)$ is of the same scaling form as Eq. (16) with $\delta \simeq 1/3$ (Fig. 9, Table I). These results verify that Eq. (19) is true for the antiadvection dynamics. As in the KPZ advection case, we can use the scaling form of $P(n,L)$ to show that $G(0,L) \sim L^{\delta}$, which, as before is borne out independently from the numerics. The function $f(y)$ seems to fit a power law $y^{-\gamma}$ with $\gamma \simeq 1.7$ (Table I) for small values of y. The singular part $P(0,L)$ satisfies $N_{occ} \equiv [1-P(0,L)]L \sim L^{\phi}$ with $\phi \simeq 0.9$, plugging this value of ϕ in Eq. (20) leads to $\gamma \simeq 1.7$, which is the same as the numerical value from direct measurement. As for the advection case, we monitored the quantity $\sigma_{\mathcal{N}_n/L}/\langle \mathcal{N}_n/L \rangle$ to characterize the fluctuations in the steady state. Our data shows that this quantity is a mildly decreasing function of L, perhaps approaching a constant. Thus the fluctuations again are anomalously large.

We have also performed measurements for the dynamical quantities. The measurement of rms displacement $R(t)$ of tagged particles shows that we have the same form as in Eq. (17) above with $\chi \simeq 1$ and $z \simeq 1.75$. The measurements on autocorrelation function (Fig. 10) show that $G(t,L)$ has the same form as Eq. (18) with $z=1.75$, and $\psi=0.19$. The value of z obtained from these two measurements is different from the advection case where it is equal to the dynamic exponent for the surface $z_s=1.5$. Since the surface is the same in both cases, one would have *a priori* expected z to be the same, thus an increase in z is surprising. It indicates that the particles do not strictly follow the valley movements. We studied the effect of varying the parameter K on the rms displacement, first studied in Ref. [17], and find that z appears to increase continuously as we decrease K; as was found in Ref. [17]. The dynamic exponent approaches the value $z=2$ as K approaches zero, which is the free random walker limit.

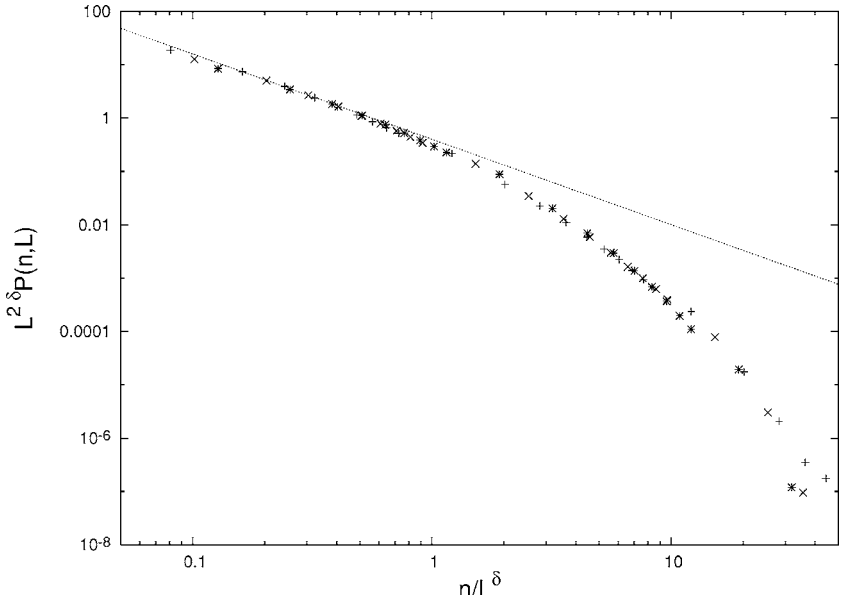

FIG. 9. The plot shows $L^{2\delta}P(n,L)$ plotted vs n/L^{δ} for the case of KPZ antiadvection, for various values of L. The value of δ is 1/3. The lattice sizes are $L=512$ (∗), 1024 (×), and 2048 (+). The straight line shows a power law with exponent −1.7

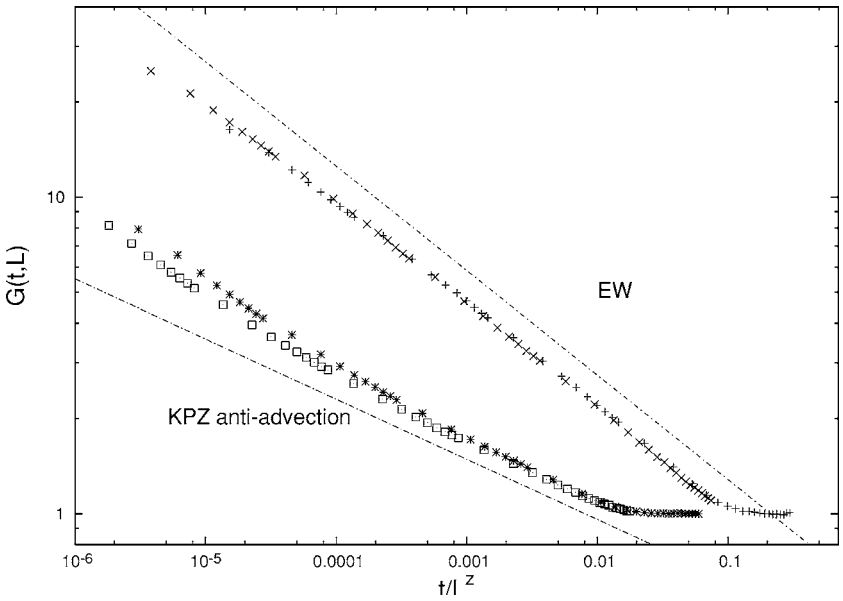

FIG. 10. $G(t,L)$ plotted vs t/L^z. $z=2$ for EW and $z=1.75$ for KPZ antiadvection dynamics. The straight lines are power laws $\tilde{Y}(\tilde{y}) \sim \tilde{y}^{-\psi}$ with $\psi=1/3$ for EW and $\psi=0.19$ for KPZ antiadvection dynamics. The lattice sizes are $L=256$ (∗, +) and 512 (×, □).

To observe the effect of varying the surface and particle update time speeds, we varied the parameter ω in the regime $1/5 \leqslant \omega \leqslant 5$. Our results indicate that the same scaling form and exponents, as described above, are valid for large system sizes and thus are universal. We see no significant crossover effects in the range of values of ω that we studied. To summarize, for antiadvection, we observe that the steady state is an SCS and as expected, the clustering is lower than in the advection case.

C. Edwards-Wilkinson surface

We now consider particles sliding on a one-dimensional surface governed by the Edwards-Wilkinson (EW) equation. This equation does not contain the up-down symmetry breaking nonlinear term and thus advection and antiadvection cases are equivalent. The absence of the nonlinear term has important consequences and it is known that the EW surface is described by exponents which differ from those of the KPZ surface. However, it is also known that in one dimension, the steady state measure of surface configurations is the same for KPZ and EW surfaces. Thus the roughness exponent for the two surfaces is the same in one dimension though the dynamic exponent is different [32]. We measured the steady state properties of the particles and saw that the steady state for the EW surface is again an SCS, which, however, lies in a different universality class from the KPZ surface. The values of the exponents indicate that the clustering in this case is less than for KPZ advection but more than for antiadvection.

The two point correlation function shows behavior similar to the previous two cases with $\theta=0$, $\nu \simeq 2/3$ (Fig. 8, Table I). The probability distribution of density again has a similar scaling form as before and $\delta \simeq 2/3$ (Fig. 11, Table I). Our results show that $\delta=\nu-\theta$ and that the singular part of the scaling function scales as $G(0,L) \sim L^{\delta}$ as for the KPZ advec-

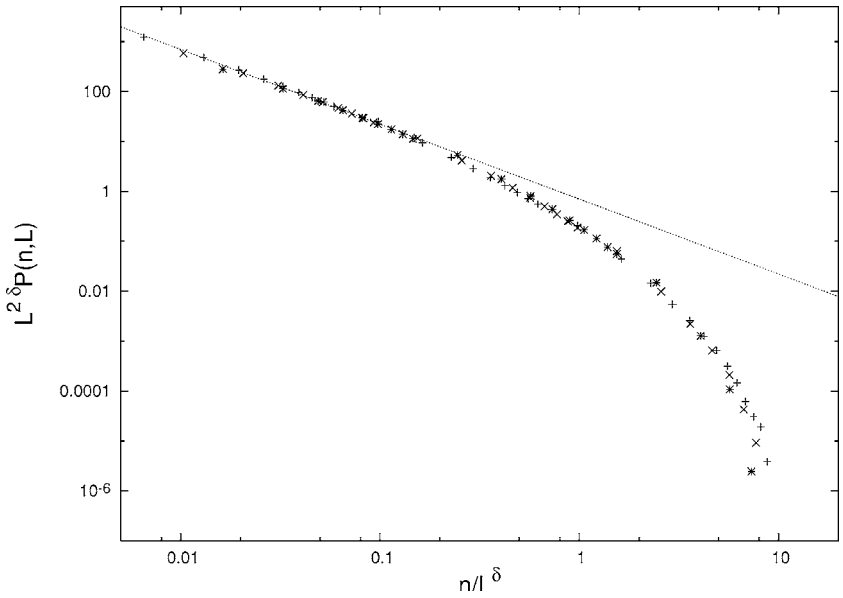

FIG. 11. The plot shows $L^{2\delta}P(n,L)$ plotted vs n/L^{δ} for the EW case for various values of L. The value of δ is 2/3. The lattice sizes are $L=512$ (∗), 1024 (×), and 2048 (+). The straight line shows a power law with exponent −1.49.

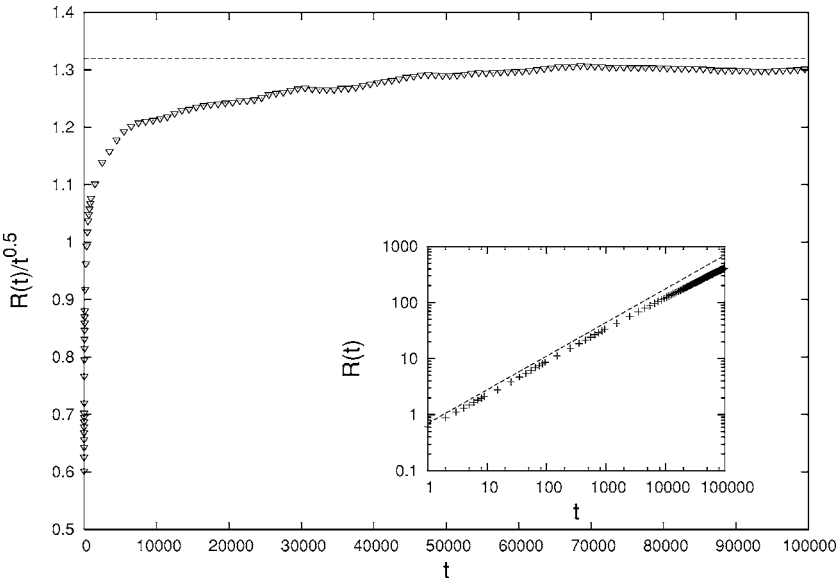

FIG. 12. The main figure shows that for EW dynamics with $\omega=2$, the ratio $R(t)/t^{1/2}$ approaches a constant (dotted straight line) at large t, indicating that the larger value 0.6 (see inset) is only an effective exponent at small times.

tion and antiadvection cases. The functional form for $f(y)$ again fits a power law $y^{-\gamma}$ for small y, $\gamma \simeq 1.49$ (Table I). We have for $P(0,L)-N_{occ} \equiv [1-P(0,L)]L \sim L^{\phi}$ with $\phi \simeq 0.75$ and Eq. (20) leads to $\gamma \simeq 1.62$, close to our numerical value from the data for $P(n,L)$. Our data for $\sigma_{\mathcal{N}_n/L}/\langle \mathcal{N}_n/L \rangle$ in steady state again indicates the presence of strong fluctuations.

Our measurements on the dynamical quantities (Fig. 10) show that $z \simeq 2$ and $\psi \simeq 1/3$. The dynamic exponent for the EW surface $z_s=2$ and thus one can conclude that the particles follow the valley movements. The system is similar to the KPZ advection in this regard. We measured the static and dynamic quantities in the range $1/5 \leqslant \omega \leqslant 5$ and observe that the SCS survives and the exponents describing the static quantities remain unchanged. Regarding the dynamical exponent, an earlier work [27] suggested that there might well be two different values of z in the two regimes $\omega \leqslant 1 (z=2)$ and $\omega > 1 (z<2)$, but the possibility remained that this is a crossover effect. In order to answer this, we performed Monte Carlo simulations (Fig. 12). We conclude that the apparent change in the dynamic exponent is indeed a transient phenomenon. The inset in Fig. 12 shows that the power law $R(t) \sim t^{0.6}$ seems to fit the data well at relatively low times while the main figure shows that if the data is divided by $t^{1/2}$, the resulting curve approaches a flat line at large times indicating that $R(t) \sim t^{1/2}$ at large times.

We infer from the above results that the steady state is an SCS for all three kinds of dynamics under consideration. The divergence of the correlation function is the strongest for the KPZ advection case followed by EW and the KPZ antiadvection cases indicating that the amount of clustering also decreases in that order. This can be seen visually in Fig. 13. Furthermore, the SCS survives under the variation of ω and the value of the exponent characterizing clustering remains the same, indicating universality of the exponents. In the KPZ advection and the EW cases, the dynamic exponent characterizing the motion of the particles is the same in numerical value as the dynamic exponent characterizing surface motion, indicating a tendency of the particles to follow the valley movement. The antiadvection case in this regard shows puzzling behavior with different dynamic exponent values for the particle and surface motion.

IV. A RELATED EQUILIBRIUM PROBLEM

Let us now consider the static surface limit, $\omega \to 0$, for the three kinds of dynamics considered above. As we discussed briefly in the Introduction, this limit does not commute with the limit $L \to \infty$. In the numerical results described above, we have seen that as we go to smaller values of ω, the steady state remains the nonequilibrium SCS with the same exponents as for $\omega=1$. Thus the $L \to \infty$ limit followed by the $\omega \to 0$ leads to the nonequilibrium steady state SCS.

We are now interested in the reverse limit, $\omega \to 0$ followed by $L \to \infty$. In this limit, the surface is stationary. The particles move on this static surface under the effect of noise. A typical time scale of particle motion $\tau \sim e^{A\sqrt{L}}$ is the time in which the particles cross the largest hills in the landscape. In this adiabatic limit, the problem becomes a well-known equilibrium problem—the Sinai model [23] for random walkers on a random landscape. It is well-known that for the KPZ and the EW surfaces in one-dimension, the distribution of heights $h(r)$ in the stationary state is described by

$$\text{Prob}[\{h(r)\}] \propto \exp\left[-\frac{\nu}{2D_h}\int \left(\frac{dh(r')}{dr'}\right)^2 dr'\right]. \quad (24)$$

Thus any stationary configuration can be thought of as the trace of a random walker in space evolving via the equation, $dh(r)/dr=\xi(r)$ where the white noise $\xi(r)$ has zero mean and is delta correlated, $\langle \xi(r)\xi(r') \rangle = \delta(r-r')$. We impose periodic boundary conditions as for the lattice model, without loss of generality—$h(0)=h(L)=0$.

The passive particles moving on top of this surface, as we remember, move according to Eq. (2). Since this is an equilibrium situation, $\langle \zeta_m(t)\zeta_m(t') \rangle = 2\kappa\delta(t-t') = 2K_B T\delta(t-t')$ where T is the temperature and K_B is the Boltzmann constant. Since the particles are noninteracting, we can deal with

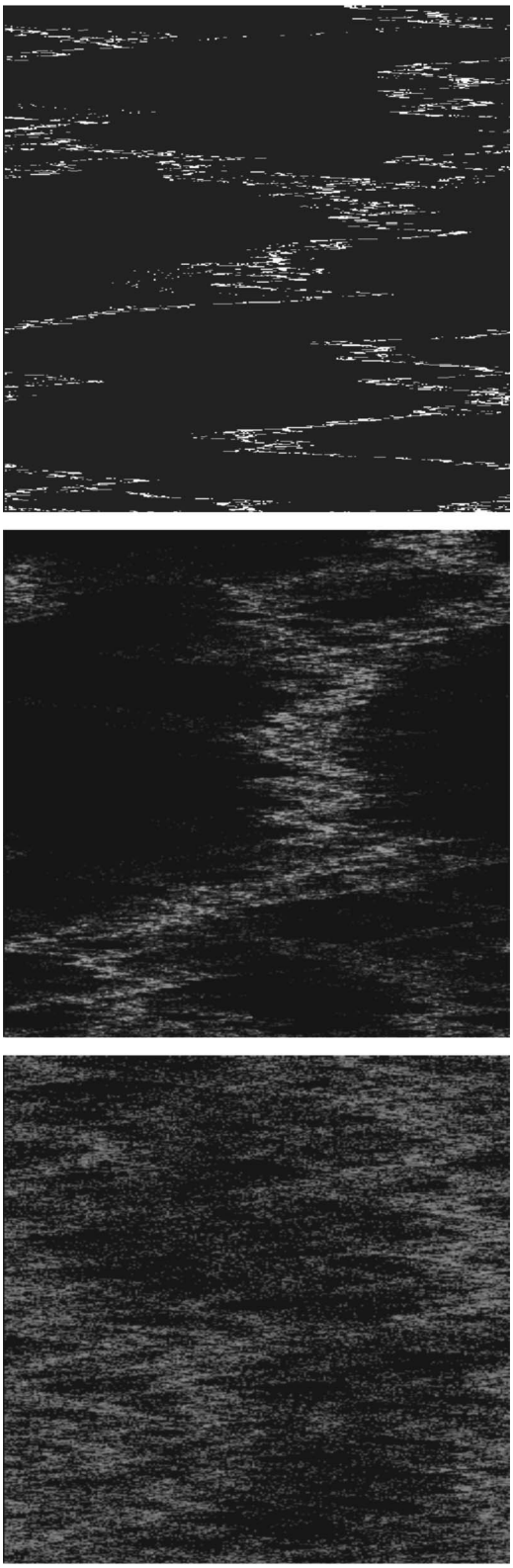

FIG. 13. Time evolution for the KPZ advection, EW and KPZ antiadvection dynamics (from up to down). The vertical axis shows time and the horizontal axis shows the one-dimensional lattice. The white spots show the presence of particles. The lattice size and the number of particles are both 256 for all three cases, so fewer white spots indicate a higher degree of clustering (fewer but more dense clusters).

a single particle and instead of the number of particles n_r at a site r, we consider the probability $\rho(r)dr$ that the particle will be located between r and $r+dr$. In the long time, the particle will reach its thermal equilibrium in the potential $h(r)$ and will be distributed according to the Gibbs-Boltzmann distribution,

$$\rho(r) = \frac{e^{-\beta h(r)}}{Z}, \tag{25}$$

where $Z=\int_0^L dr e^{-\beta h(r)}$ is the partition function. Note that $\rho(r)$ in Eq. (25) depends on the realization of the potential $\{h(r)\}$ and varies from one realization to another. Our goal would be to compute the distribution of $\rho(r)$ over different realizations of the random potential $h(r)$ drawn from the distribution in Eq. (24). Note that the distribution of $h(r)$ in Eq. (24) is invariant under the transformation $h(r) \to -h(r)$. In other words, the equilibrium density $\rho(r)$ defined in Eq. (25) will have the same distribution if one changes the sign of $h(r)$ in Eq. (25). For later simplicity, we will make this transformation now and replace $\rho(r)$ instead by the following definition:

$$\rho(r) = \frac{e^{\beta h(r)}}{Z}, \tag{26}$$

where the transformed partition function is now given by $Z = \int_0^L dr e^{\beta h(r)}$.

A. The exact distribution of the probability density

Our strategy would be first to compute the nth moment of the random variable $\rho(r)$ in Eq. (26). It follows from Eq. (26):

$$\rho^n(r) = \frac{e^{n\beta h(r)}}{Z^n} = \frac{1}{\Gamma(n)} \int_0^\infty dy y^{n-1} e^{-yZ+n\beta h(r)}, \tag{27}$$

where we have used the identity $\int_0^\infty dy y^{n-1} e^{-yZ} = \Gamma(n)/Z^n$ to rewrite the factor $1/Z^n$. Here $\Gamma(n)$ is the standard gamma function. Next, we make a further change of variable in Eq. (27) by writing $y=\beta^2 e^{\beta u}/2$. Note that as y varies from 0 to ∞, the new dummy variable u varies from $-\infty$ to ∞. Making this substitution in Eq. (27) we get

$$\rho^n(r) = b_n \int_{-\infty}^{\infty} du \exp\left[-\frac{\beta^2}{2} \left\{ \int_0^L dx e^{\beta(h(x)+u)} \right\} + n\beta[h(r)+u] \right], \tag{28}$$

where we have used the explicit expression of the partition function, $Z=\int_0^L dr e^{\beta h(r)}$. The constant $b_n = \beta^{2n+1}/[2^n \Gamma(n)]$. We are now ready to average the expression in Eq. (28) over the disorder, i.e., all possible realizations of the random potential $h(x)$ drawn from the distribution in Eq. (24). Taking the average in Eq. (28) (we denote it by an overbar), we get using Eq. (24)

$$\overline{\rho^n(r)} = Ab_n \int_{-\infty}^{\infty} du \int_{h(0)=0}^{h(L)=0} \mathcal{D}h(x) \times \exp\left[-\left\{ \int_0^L dx \left[\frac{1}{2}\left(\frac{dh(x)}{dx}\right)^2 + \frac{\beta^2}{2} e^{\beta(h(x)+u)} \right] \right\} + n\beta[h(r)+u] \right], \tag{29}$$

where the normalization constant A of the path integral in Eq. (29) will be chosen so as to satisfy the sum rule, $\int_0^L \overline{\rho(r)} dr = 1$. Next we shift the potential by a constant amount u, i.e., we define a new function $V(x) = h(x) + u$ for all x that reduces Eq. (29) to the following expression:

$$\overline{\rho^n(r)} = Ab_n \int_{-\infty}^{\infty} du \int_{V(0)=u}^{V(L)=u} \mathcal{D}V(x) \times \exp\left[-\left\{ \int_0^L dx \left[\frac{1}{2}\left(\frac{dV(x)}{dx}\right)^2 + \frac{\beta^2}{2} e^{\beta V(x)} \right] \right\} + n\beta V(r) \right]. \tag{30}$$

This path integral can be viewed as a quantum mechanical problem in the following sense. All paths (with the measure shown above) start from $V(0) = u$ and end at $V(L) = u$. At the fixed point r (where we are trying to calculate the density distribution), these paths take a value $V(r) = V$ which can vary from $-\infty$ to ∞. This can be written, using the quantum mechanical bra-ket notation,

$$\overline{\rho^n(r)} = Ab_n \int_{-\infty}^{\infty} du \int_{-\infty}^{\infty} dV \langle u | e^{-\hat{H}r} | V \rangle e^{n\beta V} \times \langle V | e^{-\hat{H}(L-r)} | u \rangle. \tag{31}$$

The first bra-ket inside the integral in Eq. (31) denotes the propagation of paths from the initial value u to V at the intermediate point r and the second bra-ket denotes the subsequent propagation of the paths from V at r to the final value u at L. The Hamiltonian $\hat{H}$ corresponds to the operator $\hat{H} \equiv \frac{1}{2}(\frac{dV}{dx})^2 + \frac{\beta^2}{2} e^{\beta V(x)}$. Interpreting $V(x)$ to be the "position" of a fictitious particle at the fictitious "time" x, this operator has a standard kinetic energy term and a potential energy which is exponential in the "position" V. The right-hand side of Eq. (31) can be rearranged and simplified as in the following:

$$\overline{\rho^n(r)} = Ab_n \int_{-\infty}^{\infty} dV e^{n\beta V} \int_{-\infty}^{\infty} du \langle V | e^{-\hat{H}(L-r)} | u \rangle \times \langle u | e^{-\hat{H}r} | V \rangle. \tag{32}$$

Thus

$$\overline{\rho^n(r)} = Ab_n \int_{-\infty}^{\infty} dV e^{n\beta V} \langle V | e^{-\hat{H}L} | V \rangle, \tag{33}$$

where we have used the completeness condition, $\int_{-\infty}^{\infty} du |u\rangle\langle u| = \hat{I}$ with $\hat{I}$ being the identity operator. At this point, it may be helpful and less confusing notationally if we denote the "position" V of the fictitious quantum particle by a more friendly notation $V \equiv X$, which will help us in thinking more clearly. Thus Eq. (33) then reduces to

$$\overline{\rho^n(r)} = Ab_n \int_{-\infty}^{\infty} dX e^{n\beta X} \langle X | e^{-\hat{H}L} | X \rangle. \tag{34}$$

To evaluate the matrix element in Eq. (34), we need to know the eigenstates and the eigenvalues of the Hamiltonian operator $\hat{H}$. It is best to work in the "position" basis X. In this basis, the eigenfunctions $\psi_E(X)$ of $\hat{H}$ satisfies the standard Shrödinger equation,

$$-\frac{1}{2}\frac{d^2\psi_E(X)}{dX^2} + \frac{\beta^2}{2} e^{\beta X} \psi_E(X) = E\psi_E(X), \tag{35}$$

valid in the range $-\infty < X < \infty$. It turns out that this Schrödinger equation has no bound state ($E < 0$) and only has scattering states with $E \geqslant 0$. We label these positive energy eigenstates by $E = \beta^2 k^2/8$, where k is a continuous label varying from 0 to ∞. A negative k eigenfunction is the same as the positive k eigenfunction, and hence it is counted only once. With this labeling, it turns out that the differential equation can be solved and one finds that the eigenfunction $\psi_k(X)$ is given by

$$\psi_k(X) = a_k K_{ik}(2e^{\beta X/2}), \tag{36}$$

where $K_\nu(y)$ is the modified Bessel function with index ν. Note that, out of two possible solutions of the differential equation, we have chosen the one which does not diverge as $X \to \infty$, one of the physical boundary conditions. The important question is: how to determine the constant a_k in Eq. (36)? Note that, unlike a bound state, the wave function $\psi_k(X)$ is not normalizable. To determine the constant a_k, we examine the asymptotic behavior of the wave function in the regime $X \to -\infty$. Using the asymptotic properties of the Bessel function (when its argument $2e^{\beta X/2} \to 0$), we find that

$$\psi_k(X) \to a_k \left[\frac{\Gamma(ik)}{2} e^{-ik\beta X/2} - \frac{\pi}{2\sin(ik\pi)\Gamma(1+ik)} e^{ik\beta X/2} \right]. \tag{37}$$

On the other hand, in the limit $X \to -\infty$, the Schrödinger equation (35) reduces to a free problem,

$$-\frac{1}{2}\frac{d^2\psi_k(X)}{dX^2} = \frac{\beta^2 k^2}{8}\psi_k(X), \tag{38}$$

which allows plane wave solutions of the form

$$\psi_k(X) \approx \sqrt{\frac{\beta}{4\pi}} [e^{ik\beta X/2} + r(k) e^{-ik\beta X/2}], \tag{39}$$

where $e^{ik\beta X/2}$ represents the incoming wave from $X = -\infty$ and $e^{-ik\beta X/2}$ represents the reflected wave going back towards $X = -\infty$ with $r(k)$ being the reflection coefficient. The amplitude $\sqrt{\frac{\beta}{4\pi}}$ is chosen such that the plane waves $\psi_k(X) = \sqrt{\frac{\beta}{4\pi}} e^{ik\beta X/2}$ are properly orthonormalized in the sense that $\langle \psi_k | \psi_{k'} \rangle = \delta(k - k')$ where $\delta(z)$ is the Dirac delta function. Comparing Eqs. (37) and (39) in the regime $X \to -\infty$, we determine the constant a_k (up to a phase factor),

$$a_k = \sqrt{\frac{\beta}{\pi^3}} \sin(ik\pi)\Gamma(1+ik). \tag{40}$$

The square of the amplitude $|a_k|^2$ (which is independent of the unknown phase factor) is then given by

$$|a_k|^2 = \frac{\beta k \sinh(\pi k)}{\pi^2}, \tag{41}$$

where we have used the identity, $\Gamma(1+ik)\Gamma(1-ik) = \pi k/\sinh(\pi k)$. Therefore the eigenstates of the operator $\hat{H}$ are given by $|k\rangle$, such that $\hat{H}|k\rangle = \frac{\beta^2 k^2}{8}|k\rangle$ and in the X basis, the wave function $\psi_k(X) = \langle k|X\rangle$ is given (up to a phase factor) by the exact expression

$$\psi_k(X) = \frac{\sqrt{\beta k \sinh(\pi k)}}{\pi} K_{ik}(2e^{\beta X/2}). \tag{42}$$

We now go back to Eq. (34) where we are ready to evaluate the matrix element $\langle X|e^{-\hat{H}L}|X\rangle$ given the full knowledge of the eigenstates of $\hat{H}$. Expanding all the kets and bras in the eigenbasis $|k\rangle$ of $\hat{H}$, we can rewrite Eq. (34) as follows:

$$\overline{\rho^n(r)} = Ab_n \int_{-\infty}^{\infty} dX \int_0^{\infty} dk \langle X|k\rangle\langle k|X\rangle \times e^{n\beta X} e^{-\beta^2 k^2 L/8}$$

$$= Ab_n \int_0^{\infty} dk e^{-\beta^2 k^2 L/8} \int_{-\infty}^{\infty} dX |\psi_k(X)|^2 e^{n\beta X}. \tag{43}$$

The X integral on the right-hand side of Eq. (43) can be expressed in a compact notation,

$$\int_{-\infty}^{\infty} dX |\psi_k(X)|^2 e^{n\beta X} = \langle k|e^{n\beta \hat{X}}|k\rangle. \tag{44}$$

Substituting the exact form of $\psi_k(X)$ from Eq. (42), we get

$$\langle k|e^{n\beta\hat{X}}|k\rangle = \frac{k \sinh(\pi k)}{\pi^2 2^{2n-1}} \int_0^{\infty} dy y^{2n-1} K_{ik}(y) K_{-ik}(y). \tag{45}$$

Fortunately, the integral on the right-hand side of Eq. (45) can be done in closed form [33] and we obtain,

$$\langle k|e^{n\beta\hat{X}}|k\rangle = \frac{k \sinh(\pi k)}{\pi^2 2^{2n-1}} \frac{\Gamma^2(n)}{\Gamma(2n)} \Gamma(n-ik)\Gamma(n+ik). \tag{46}$$

Substituting this matrix element back in Eq. (43), we arrive at our final expression,

$$\overline{\rho^n(r)} = A \frac{\beta^{2n+1}}{4\pi^2 2^n} \frac{\Gamma(n)}{\Gamma(2n)} \int_0^{\infty} dk k \sinh(\pi k)$$

$$\times |\Gamma(n-ik)|^2 e^{-\beta^2 k^2 L/8}. \tag{47}$$

To determine the constant A, we first put $n=1$ in Eq. (47). Note that $\overline{\rho(r)} = 1/L$ by virtue of the probability sum rule, $\int_0^L \rho(r)dr = 1$. Taking the disorder average and using the translational invariance, one gets $\overline{\rho(r)} = 1/L$. Using the identity, $\Gamma(1+ik)\Gamma(1-ik) = \pi k/\sinh(\pi k)$ and performing the integral on the right-hand side of Eq. (47) and then demanding that the right-hand side must equal $1/L$ for $n=1$, we get

$$A = \sqrt{2\pi L}. \tag{48}$$

One can also check easily that $n \to 0$, the right-hand side of Eq. (47) approaches to 1 as it should. In verifying this limit, we need to use the fact that $\Gamma(x) \approx 1/x$ as $x \to 0$ and also the identity, $\Gamma(ik)\Gamma(-ik) = \pi/k \sinh(\pi k)$. Now, for $n > 0$ (strictly), one can make a further simplification of the right-hand side of Eq. (47). We use the property of the gamma function, $\Gamma(x+1) = x\Gamma(x)$, repeatedly to write $\Gamma(n-ik) = (n-1-ik)\Gamma(n-1-ik) = (n-1-ik)(n-2-ik)\cdots(1-ik)\Gamma(1-ik)$. Note that this formula, so far, is valid only for integer $n \geqslant 1$. This gives, for integer $n \geqslant 1$

$$\Gamma(n-ik)\Gamma(n+ik) = [(n-1)^2 + k^2]$$

$$\times [(n-2)^2 + k^2] \cdots \times [1+k^2] \frac{\pi k}{\sinh(\pi k)}, \tag{49}$$

where we have used the identity $\Gamma(1+ik)\Gamma(1-ik) = \pi k/\sinh(\pi k)$. Substituting this expression in Eq. (47) we get, for $n \geqslant 1$,

$$\overline{\rho^n(r)} = \sqrt{2\pi L} \frac{\beta^{2n+1}}{4\pi 2^n} \frac{\Gamma(n)}{\Gamma(2n)} \int_0^{\infty} dk k^2 [(n-1)^2 + k^2]$$

$$\times [(n-2)^2 + k^2] \cdots [1+k^2] e^{-\beta^2 k^2 L/8}. \tag{50}$$

Making the change of variable $\beta^2 k^2 L/8 = z$ in the integral, we finally obtain the following expression for all integer $n \geqslant 1$:

$$\overline{\rho^n(r)} = \frac{1}{L\sqrt{\pi}} \frac{\beta^{2n-2}}{2^{n-2}} \frac{\Gamma(n)}{\Gamma(2n)} \int_0^{\infty} dz e^{-z} z^{1/2} \left[1^2 + \frac{8z}{\beta^2 L}\right]$$

$$\times \left[2^2 + \frac{8z}{\beta^2 L}\right] \cdots \left[(n-1)^2 + \frac{8z}{\beta^2 L}\right]. \tag{51}$$

For example, consider the case $n=2$. In this case, the formula in Eq. (51) gives

$$\overline{\rho^2(r)} = \frac{\beta^2}{12L}\left[1 + \frac{12}{\beta^2 L}\right], \tag{52}$$

which is valid for all L and not just for large L. Note that the second term on the right-hand side gives a contribution which is exactly $1/L^2$. This means that the variance, $\overline{\rho^2(r)} - \overline{\rho(r)}^2 = \beta^2/[12L]$ for all L. For arbitrary integer $n \geqslant 1$, taking the large L limit in Eq. (51) we get, as $L \to \infty$,

$$\overline{\rho^n(r)} \to \frac{1}{L}\left[\frac{\beta^{2n-2}}{2^{n-2}} \frac{\Gamma^3(n)}{\Gamma(2n)}\right]. \tag{53}$$

Note that even though this expression was derived assuming integer $n \geqslant 1$, after obtaining this formula, one can analytically continue it for all noninteger $n > 0$. Now, let us denote $\text{Prob}(\rho, L) = P(\rho, L)$. Then $\overline{\rho^n(r)} = \int_0^{\infty} \rho^n P(\rho, L) d\rho$. Note again that the range of ρ is from 0 to ∞, since it is a probability density, and not a probability. The factor $1/L$ on the right-hand side of Eq. (53) suggests that $P(\rho, L)$ has the following behavior for large L:

$$P(\rho,L) = \frac{1}{L} f_0(\rho), \tag{54}$$

where the function $f_0(y)$ satisfies the equation

$$\int_0^\infty y^n f_0(y) dy = \left[\frac{\beta^{2n-2}}{2^{n-2}} \frac{\Gamma^3(n)}{\Gamma(2n)} \right]. \tag{55}$$

To determine $f_0(y)$ from this equation, we first use the identity, $\Gamma(2n) = 2^{2n-1}\Gamma(n)\Gamma(n+1/2)/\sqrt{\pi}$, known as the doubling formula for the gamma function. Next we use [34]

$$\int_0^\infty x^{n-1} e^{-ax} K_0(ax) dx = \frac{\sqrt{\pi}}{(2a)^n} \frac{\Gamma^2(n)}{\Gamma(n+1/2)}. \tag{56}$$

Identifying the right-hand side of Eq. (56) with the right-hand side of Eq. (55) upon choosing $a = 2/\beta^2$, we get the exact expression of $f_0(y)$,

$$f_0(y) = \frac{2}{\beta^2 y} e^{-2y/\beta^2} K_0\left(\frac{2y}{\beta^2} \right). \tag{57}$$

More cleanly, we can then write that for large L,

$$P(\rho,L) = \frac{4}{\beta^4 L} f_1\left[\frac{2\rho}{\beta^2} \right], \tag{58}$$

where the scaling function $f_1(y)$ is universal (independent of the system parameter β) and is given by

$$f_1(y) = \frac{e^{-y}}{y} K_0(y). \tag{59}$$

This function has the following asymptotic behaviors:

$$f_1(y) \approx \begin{cases} \frac{1}{y}[-\ln(y/2) + 0.5772\ldots], & y \to 0, \\ \sqrt{\frac{\pi}{2y^3}} e^{-2y}, & y \to \infty. \end{cases} \tag{60}$$

The scaling form in Eq. (58) is valid only when $n(r) \sim L$. If $n(r)$ is a number of order $O(1)$ (not as large as L), then the scaling breaks down. This fact suggests that the correct behavior of the distribution $P(\rho,L)$ for large L actually has two parts,

$$P(\rho,L) \approx \left[1 - \frac{\ln^2(L)}{\beta^2 L} \right] \delta(\rho) + \frac{4}{\beta^4 L} f_1\left[\frac{2\rho}{\beta^2} \right] \theta\left(\rho - \frac{c}{L} \right), \tag{61}$$

where $f_1(y)$ is given by Eq. (59). This form in Eq. (61) is consistent with all the observed facts. For example, if one integrates the right-hand side, the first term gives $1 - \frac{\ln^2(L)}{\beta^2 L}$ [with the convention $\int_0^\infty \delta(y) dy = 1$]. The second term, when integrated, gives $\frac{\ln^2(L)}{\beta^2 L}$ [where we have used the small y behavior of $f_1(y)$ from Eq. (60) and kept only the leading order term for large L] which exactly cancels the identical factor in the first term to give a total sum 1, as it should. On the other hand, for any finite moment of order n, the first term does not contribute and only the second term contributes to give the result in Eq. (53).

B. The density-density correlation function

We now consider the density-density correlation function between two points r_1 and r_2 at equilibrium. The calculation proceeds more or less along the same lines as in the previous section. The density-density correlation function is defined as

$$C(r_1,r_2) = \overline{\rho(r_1)\rho(r_2)}, \tag{62}$$

which evidently depends only on $r = |r_1 - r_2|$ due to the translational invariance. The density $\rho(r)$ is again given by Eq. (26). It follows from Eq. (26) that

$$\rho(r_1)\rho(r_2) = \frac{e^{\beta[h(r_1)+h(r_2)]}}{Z^2} = \int_0^\infty dy y e^{-yZ + \beta[h(r_1)+h(r_2)]}, \tag{63}$$

where the partition function $Z = \int_0^L dr e^{\beta U(r)}$ and we have used the identity $1/Z^2 = \int_0^\infty dy y e^{-Zy}$. As in the previous section, we now make a change of variable in Eq. (63) by writing $y = \beta^2 e^{\beta u}/2$. Then Eq. (63) becomes

$$\rho(r_1)\rho(r_2) = \frac{\beta^5}{4} \int_{-\infty}^\infty du \exp\left[-\frac{\beta^2}{2} \left\{ \int_0^L dx e^{\beta[h(x)+u]} \right\} + \beta[h(r_1) + u + h(r_2) + u] \right], \tag{64}$$

where we have used the explicit expression of the partition function, $Z = \int_0^L dr e^{\beta h(r)}$. Averaging over the disorder, we get

$$\overline{\rho(r_1)\rho(r_2)} = B \frac{\beta^5}{4} \int_{-\infty}^\infty du \int_{h(0)=0}^{h(L)=0} \mathcal{D}h(x) \times \exp\left[-\left\{ \int_0^L dx \times \frac{1}{2}\left(\frac{dh(x)}{dx} \right)^2 \left[\frac{1}{2}\left(\frac{dh(x)}{dx} \right)^2 + \frac{\beta^2}{2} e^{\beta[h(x)+u]} \right] \right\} + \beta[h(r_1) + h(r_2) + 2u] \right], \tag{65}$$

where the normalization constant B will be determined from the condition, $\int_0^L \int_0^L C(r_1,r_2) dr_1 dr_2 = 1$ [which follows from the fact that $\int_0^L \rho(r) dr = 1$]. Alternatively, one can put $r = r_2 - r_1 = 0$ in the expression for the correlation function and then it should be the same as $\overline{\rho^2(r)}$ already computed in the previous section.

As before, we next shift the potential, i.e., we define $V(x) = U(x) + u$ for all x. Equation (65) then simplifies,

$$\overline{\rho(r_1)\rho(r_2)} = B \frac{\beta^5}{4} \int_{-\infty}^\infty du \int_{V(0)=u}^{V(L)=u} \mathcal{D}V(x) \times \exp\left[-\left\{ \int_0^L dx \left[\frac{1}{2}\left(\frac{dV(x)}{dx} \right)^2 + \frac{\beta^2}{2} e^{\beta V(x)} \right] \right\} + \beta[V(r_1) + V(r_2)] \right]. \tag{66}$$

Thus we have again reduced the problem to a path integral problem. However, there is a difference in the subsequent calculations. This is because, unlike the previous calculation, we now have to divide the paths into three parts: (i) paths

starting at $V(0)=u$ and propagating up to the point r_1 where $V(r_1)=V_1$ (note that V_1 can vary from $-\infty$ to ∞), (ii) paths starting at r_1 with $V(r_1)=V_1$ and propagating up to r_2 with $V(r_2)=V_2$, and (iii) paths starting at r_2 with $V(r_2)=V_2$ and propagating up to L where $V(L)=u$. We have assumed $r_2 \geqslant r_1$ for convenience. Using the bra-ket notation, we can then rewrite Eq. (66) as

$$\overline{\rho(r_1)\rho(r_2)} = B\frac{\beta^5}{4}\int_{-\infty}^{\infty} du \int_{-\infty}^{\infty} dV_1 \int_{-\infty}^{\infty} dV_2 \times \langle u|e^{-\hat{H}r_1}|V_1\rangle e^{\beta V_1}\langle V_1|e^{-\hat{H}(r_2-r_1)}|V_2\rangle \times e^{\beta V_2}\langle V_2|e^{-\hat{H}(L-r_2)}|u\rangle. \quad (67)$$

The Hamiltonian $\hat{H} \equiv \frac{1}{2}\left(\frac{dV}{dx}\right)^2 + \frac{\beta^2}{2}e^{\beta V(x)}$ is the same as in the previous section. Using $\int_{-\infty}^{\infty} du|u\rangle\langle u| = \hat{I}$, Eq. (67) can be simplified,

$$\overline{\rho(r_1)\rho(r_2)} = B\frac{\beta^5}{4}\int_{-\infty}^{\infty} dV_1 \int_{-\infty}^{\infty} dV_2 \langle V_2|e^{-\hat{H}(L-r)}|V_1\rangle \times \langle V_1|e^{-\hat{H}r}|V_2\rangle e^{\beta(V_1+V_2)}, \quad (68)$$

where $r=r_2-r_1$. Note that Eq. (68) clearly shows that $C(r_1,r_2,L)=C(r=r_2-r_1,L)$, as it should due to the translational invariance. Furthermore, Eq. (68) also shows that function $C(r,L)$ is symmetric around $r=L/2$, i.e., $C(r,L)=C(L-r,L)$. This last fact is expected due to the periodic boundary condition. As before, we change to a more friendly notation: $V_1 \equiv X_1$ and $V_2 \equiv X_2$, where X_1 and X_2 denote the "positions" of the fictitious quantum particle at "times" r_1 and r_2. With this notation, Eq. (68) reads

$$\overline{\rho(r_1)\rho(r_2)} = B\frac{\beta^5}{4}\int_{-\infty}^{\infty} dX_1 \int_{-\infty}^{\infty} dX_2 \times \langle X_2|e^{-\hat{H}(L-r)}|X_1\rangle \times \langle X_1|e^{-\hat{H}r}|X_2\rangle e^{\beta(X_1+X_2)}. \quad (69)$$

This can be solved to obtain the correlation function

$$C(r,L) = B\frac{\beta^5}{256}\int_0^{\infty}\int_0^{\infty} dk_1 dk_2 k_1 k_2 (k_1^2-k_2^2)^2 \times \frac{\sinh(\pi k_1)\sinh(\pi k_2)}{[\cosh(\pi k_1)-\cosh(\pi k_2)]^2} \times \exp\left[-\frac{\beta^2}{8}[k_1^2(L-r)+k_2^2 r]\right]. \quad (70)$$

For $r=0$, it is possible to perform the double integral in Eq. (70) and one finds that it reduces to the expression of $\overline{\rho^2(r)}$ in Eq. (52) of the previous section, provided the normalization constant $B=\sqrt{2\pi}L$. Thus the two-point density-density correlator is given exactly by Eq. (70) (with $B=\sqrt{2\pi}L$) and note that this expression is valid for all L. This exact expression of the correlation function was first derived by Comtet and Texier [24] in the context of a localization problem in disordered supersymmetric quantum mechanics.

To extract the asymptotic behavior for large L, we rescale $k_1\sqrt{L-r}=x_1$ and $k_2\sqrt{L}=x_2$ in Eq. (70), then expand the sinh's and the cosh's for small arguments, perform the resulting double integral (which becomes simple after the expansion), and finally get for $L\to\infty$ and $r\neq 0$,

$$C(r,L) \to \frac{1}{\sqrt{2\pi\beta^2}L^{5/2}[x(1-x)]^{3/2}}, \quad (71)$$

where $x=r/L$ is the scaling variable. If we identify ρ with n/L, we can identify the expressions for $P(\rho)$ and $C(r,L)$ with the corresponding equilibrium quantities—$P(n,L)=\frac{1}{L}P(\rho)$ and $G(r,L)=L^2C(r,L)$. So, for $n \geqslant 1$ and $r \geqslant 1$

$$P(n,L) = \frac{4}{\beta^4 L^2} f_1\left[\frac{2n}{\beta^2 L}\right], \quad (72)$$

where $f_1(y)$ is given in Eq. (59), and

$$G(r,L) \to \frac{1}{\sqrt{2\pi\beta^2}L^{1/2}[x(1-x)]^{3/2}}. \quad (73)$$

C. SCS, agreement with KPZ advection

The primary result to emerge from the analytic results above is that the equilibrium state again is an SCS. The second and surprising result is that the above results describe very well the numerical data for the KPZ advection case. A fit to the functional forms shows that these equilibrium results reproduce quite well the scaling exponents and scaling functions for $G(r,L)$ and $P(n,L)$ for $n \geqslant 1$ obtained numerically for the nonequilibrium KPZ advection case with $\omega=K=1$. This can be seen in Figs. 14 and 5. However, the values of β required to fit the two quantities $G(r,L)$ and $P(n,L)$ are different. The correlation function matches with $\beta \simeq 4$ while $\beta \simeq 2.3$ describes the probability density of occupancy data. However, $P(0,L)$ (and thus N_{occ}) does not agree closely in the two cases. The equilibrium case can also be used to shed light on the dynamical properties of the nonequilibrium steady state for KPZ advection. We compared our results for $\tilde{G}(t,L)$ with the density-density autocorrelation function in the adiabatic Sinai limit $\omega \to 0$. To find $\tilde{G}(t,L)$, we simulated a surface with height field $h(r,t)$ evolving according to KPZ dynamics, and evaluated the density using the equilibrium weight $\rho(r,t)=e^{-\beta h(r,t)}/Z$. As shown in Ref. [18], the results with $\beta=4$ agree with the autocorrelation function in the nonequilibrium system, apart from an overall prefactor.

It is surprising that results in this equilibrium limit describe the nonequilibrium state so well. A partial explanation is as follows. In the nonequilibrium case, the driving force behind particle motion and clustering is the surface fluctuation while in the equilibrium case, it is the temperature. The common feature in both the cases is the exploration of the surface terrain. Thus in some region of parameter space the surface motion mimics temperature and causes the particles to redistribute in a certain way. Why the equivalent temperature for various quantities is different is not clear and deserves further study. As we have mentioned before, the steady state height distribution for both the KPZ and EW surfaces are the same and so the Sinai limit is the adiabatic

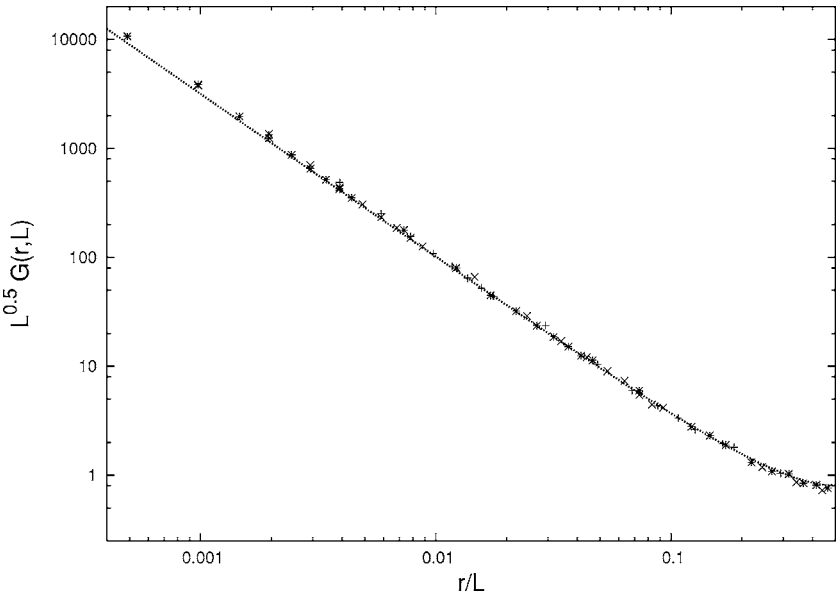

FIG. 14. The two point scaled density correlation function $G(r,L)$ (advection) for $K=1$, $\omega=1$. The line is a plot of Eq. (73) with $\beta=4$. There is a surprisingly good agreement of the nonequilibrium Monte Carlo data with the analytic equilibrium result. The lattice sizes are $L=512$ (+), 1024 (×), and 2048 (∗).

limit for all three kinds of dynamics under consideration, KPZ advection, KPZ antiadvection, and EW dynamics. However, only the KPZ advection results are well-described by the equilibrium limit.

V. TWO DIMENSIONS

In this section, we describe our results for the problem of passive sliders on fluctuating surfaces in two dimensions. Unlike in one dimension, the KPZ and EW surfaces are known to have different static properties in two dimensions. The KPZ surface, in the strong coupling regime, is known to be rough in two dimensions; the value of the roughness exponent is known to be approximately equal to 0.4 [32]. For the EW surface, it is known that the surface is only logarithmically rough and the roughness exponent is equal to zero. Apart from these facts specific to particular surfaces, we also know that there are structures like saddle points in two dimensions which may affect the particle dynamics and perhaps aid declustering. Thus, while we expect the particles to cluster in valleys, it is not *a priori* clear that the steady state will be an SCS. We performed Monte Carlo simulations on a two-dimensional lattice model, described below, to investigate the steady state and found that SCS persists even in two dimensions.

A. Lattice model in two dimensions

We consider a square lattice where the particles reside on sites and the links or bonds between successive lattice sites in the x and y directions are dynamical variables which denote local slopes of the surface as before. The total number of particles N which is taken to be equal to the total number of sites, is L^2. Each link takes either of the values +1 (upward slope $\rightarrow/$) or −1 (downward slope $\rightarrow\backslash$). A local hill in this case is a site which is at a height one unit higher than

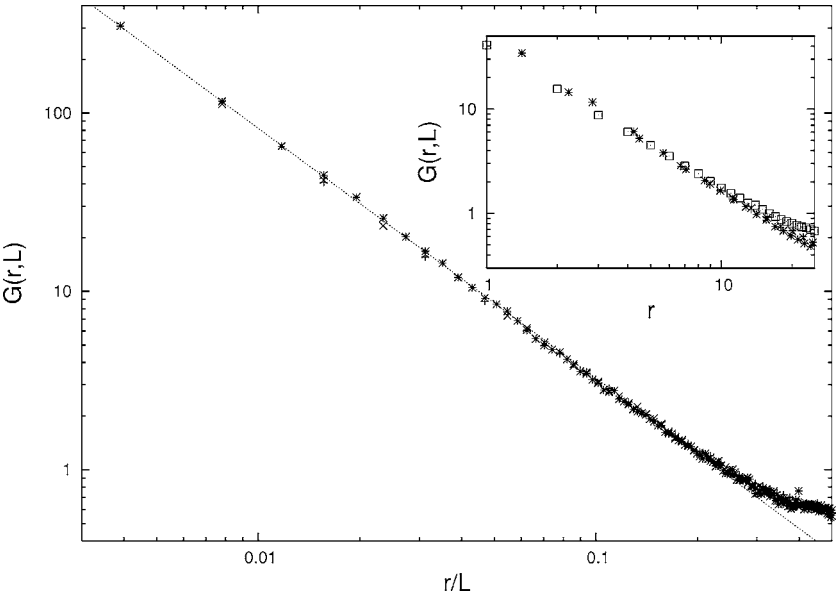

FIG. 15. The inset shows $G(r,L)$ vs r for different directions of measurement in two dimensions. The directions are characterized by the angle Θ which is measured with respect to the x axis. $\Theta=0, \pi/2$ (□), $\pi/4$ (∗), $\pi/6$ (+), and $\pi/3$ (×). We see that $G(\vec{r},L)$ is independent of the direction of measurement. The main plot shows the scaling collapse when r is scaled with L. The straight line shows a power law with exponent −1.4. The lattice sizes are $L=256$ (∗), 128 (×), and 64 (+).

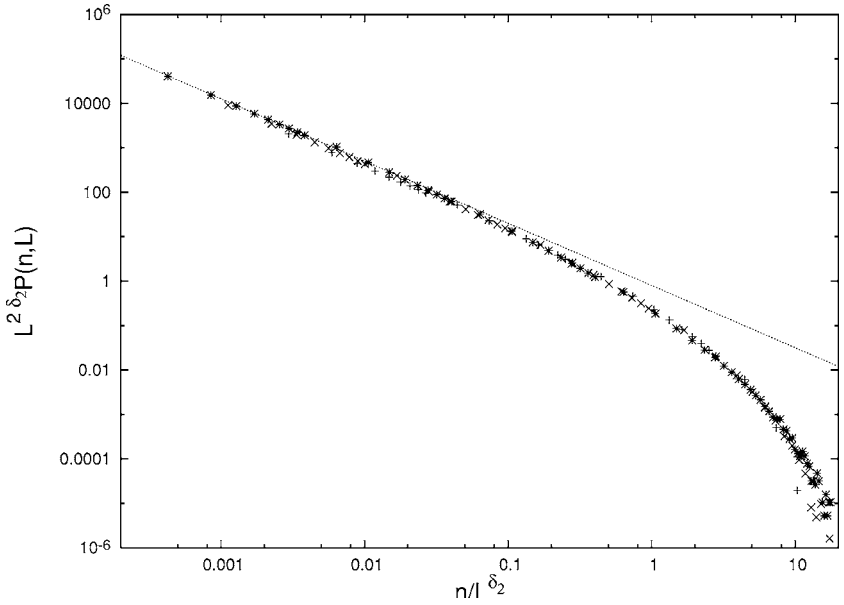

FIG. 16. The plot shows $L^{2\delta_2}P(n,L)$ plotted vs n/L^{δ_2} for the case of KPZ advection for various values of L in two dimensions. The value of δ_2 is 1.4. The lattice sizes are $L=256$ (*), 128 (×), and 64 (+). The straight line shows a power law with exponent −1.4.

all four of its nearest neighbors. In terms of slopes, one would see the configuration (Λ) in both the x and y directions. Similarly a local valley is a site which is at a height one unit lower than all four of its nearest neighbors. The rules for the surface evolution are similar to the one-dimensional ones and are based on the solid-on-solid (SOS) algorithm [35]. A site is chosen at random and if it is on a local hill, we change it to a local valley for KPZ advection dynamics. KPZ antiadvection dynamics only allows the valley to hill move and the EW dynamics allows both the moves with equal probabilities.

The particle moves are as follows. We choose a particle at random and then find out the directions which are favorable for movement, i.e., have a downward slope; we then move the particle in one of these directions chosen randomly. As before, N_p particle updates are made after every N_s surface moves and $\omega \equiv N_s/N_p$.

Our Monte Carlo simulation data shows that even in two dimensions, the steady state is an SCS and the quantities characterizing the clustering behave similarly as the one-dimension case. As in one dimension, the amount of clustering is different for the three kinds of dynamics and we see that KPZ advection dynamics shows the most clustering, followed by KPZ antiadvection, and then the EW case. This is in contrast to our results in one dimension where EW dynamics shows better clustering than the KPZ antiadvection dynamics. This can be ascribed to the fact that the surface roughness is much less for a two-dimensional EW surface ($\chi=0$) than for a strong-coupling KPZ surface ($\chi \simeq 0.4$).

B. Results

We measured the two point density-density correlation function and found that

$$G(\vec{r},L) \equiv \langle n(\vec{x})n(\vec{x}+\vec{r})\rangle_L \sim Y_2\left(\frac{r}{L}\right), \tag{74}$$

the subscript 2 in Y_2 indicating two dimensions. We see that (Fig. 15) $G(\vec{r},L)$ is independent of the direction of measurement and decays as a power law $Y_2(y) \sim y^{-\nu_2}$ with $\nu_2 \simeq 1.4$ for KPZ advection. We see similar behavior for KPZ antiadvection ($\nu_2 \simeq 0.5$) and for EW dynamics ($\nu_2 \simeq 0.3$). Thus we see that the SCS is the steady state in two dimensions as well.

We have also measured the probability distribution of occupancy $P(n,L)$. Before describing our results, we would like to mention again that we have worked with particle density equal to one, thus the total number of particles is $N=L^2$ for two dimensions ($L\times L$ lattice). $P(n,L)$ scales as

$$P(n,L) \sim \frac{1}{L^{2\delta_2}} f_2\left(\frac{n}{L^{\delta_2}}\right), \tag{75}$$

with $\delta_2 \simeq 1.4$ for KPZ advection, $\delta_2 \simeq 0.5$ for KPZ antiadvection, and $\delta_2 \simeq 0.3$ for the EW case. For the KPZ advection case, $f_2(y) \sim y^{-\gamma_2}$ with $\gamma_2 \simeq 1.4$. We can verify that Eq. (20) generalizes to $\phi_2 = \delta_2(\gamma_2 - 2) + 2$, where ϕ_2 is defined by $N_{\rm occ} \equiv (1-P(0,L))L^2 \sim L^{\phi_2}$. We obtain the value of the exponent ϕ_2 from our data for $P(0,L)$, $\phi_2 \simeq 1.37$. This leads to $\gamma_2 \simeq 1.55$, which is slightly larger than the value obtained by directly fitting a power law to $P(n,L)$.

We can do a scaling analysis and also show that $\delta_2 = \nu_2$ and that $G(0,L) = \int_0^{L^2} n^2 P(n,L) dn \sim L^{\delta_2}$ which we have verified numerically. The above equalities can be proved by using the relations $G(0,L) + \int_1^L G(r,L) r dr d\theta = L^2$ and $\int_0^{L^2} nP(n,L) = 1$.

VI. CONCLUSIONS

We have characterized the steady states of noninteracting, passive particles sliding on fluctuating surfaces. We found that the steady state of this system is a strong clustering state (SCS). This state is characterized by two properties of the density-density correlation function $G(r,L)$—it is a scaling function of distance r divided by the system size L, and the scaling function diverges near the origin. We have seen that this state is general and robust; it is present with

various kinds of surface dynamics, in one and two dimensions, and persists under a change of parameters. The other important result is the existence of an SCS in the static, equilibrium Sinai limit in one dimension. We see that not only do we get an SCS but the scaling function and the exponents match very well with our results on the nonequilibrium KPZ advection problem. This surprising result throws open interesting questions—why are two different values of β required to describe the two quantities $G(r,L)$ and $P(n,L)$? Why do only the KPZ advection case results match well with the equilibrium results when the Sinai model is the adiabatic limit for all three kind of dynamics?

ACKNOWLEDGMENTS

We thank A. Comtet for very useful discussions. S.N.M. and M.B. acknowledge support from the Indo-French Centre for the Promotion of Advanced Research (IFCPAR) under Project No. 3404-2. A.N. acknowledges support from the Kanwal Rekhi Career Development Awards.

[1] B. Drossel and M. Kardar, Phys. Rev. Lett. **85**, 614 (2000).
[2] P. Biswas, A. Majumdar, A. Mehta, and J. K. Bhattacharjee, Phys. Rev. E **58**, 1266 (1998).
[3] R. Lahiri and S. Ramaswamy, Phys. Rev. Lett. **79**, 1150 (1997); R. Lahiri, M. Barma, and S. Ramaswamy, Phys. Rev. E **61**, 1648 (2000).
[4] A. Kunwar, A. John, K. Nishinari, A. Schadschneider and D. Chowdhury, J. Phys. Soc. Jpn. **73**, 2979 (2004).
[5] B. I. Shraiman and E. D. Siggia, Nature (London) **405**, 639 (2000).
[6] G. Falkovich, K. Gawedzki, and M. Vergassola, Rev. Mod. Phys. **73**, 913 (2001).
[7] R. H. Kraichnan, Phys. Rev. Lett. **72**, 1016 (1994).
[8] D. Mitra and R. Pandit, Phys. Rev. Lett. **95**, 144501 (2005).
[9] M. R. Maxey, J. Fluid Mech. **174**, 441 (1987)
[10] E. Balkovsky, G. Falkovich, and A. Fouxon, Phys. Rev. Lett. **86**, 2790 (2001).
[11] J. M. Deutsch, J. Phys. A **18**, 1449 (1985).
[12] M. Wilkinson and B. Mehlig, Phys. Rev. E **68**, 040101(R) (2003).
[13] B. Mehlig and M. Wilkinson, Phys. Rev. Lett. **92**, 250602 (2004).
[14] V. I. Klyatskin, JETP **99**, 1005 (2004).
[15] K. Duncan, B. Mehlig, S. Ostlund, and M. Wilkinson, Phys. Rev. Lett. **95**, 240602 (2005).
[16] K. Gawedzki and M. Vergassola, Physica D **138**, 63 (2000).
[17] B. Drossel and M. Kardar, Phys. Rev. B **66**, 195414 (2002).
[18] A. Nagar, M. Barma, and S. N. Majumdar, Phys. Rev. Lett. **94**, 240601 (2005).
[19] D. Das and M. Barma, Phys. Rev. Lett. **85**, 1602 (2000).
[20] D. Das, M. Barma, and S. N Majumdar, Phys. Rev. E **64**, 046126 (2001).
[21] M. Gopalakrishnan and M. Barma, J. Stat. Phys. **110**, 1305 (2003).
[22] S. Mishra and S. Ramaswamy, cond-mat/0603051.
[23] Y. G. Sinai, Theor. Probab. Appl. **27**, 256 (1982).
[24] A. Comtet and C. Texier, *Supersymmetry and Integrable Models Proceedings, Chicago, IL*, edited by H. Aratyn, T. Imbo, W. Y. Keung, and U. Sukhatme (Springer, Berlin, 1998).
[25] T. Bohr and A. Pikovsky, Phys. Rev. Lett. **70**, 2892 (1993).
[26] C. S. Chin, Phys. Rev. E **66**, 021104 (2002).
[27] M. Gopalakrishnan, Phys. Rev. E **69**, 011105 (2003).
[28] M. Kardar, G. Parisi, and Y. C. Zhang, Phys. Rev. Lett. **56**, 889 (1986).
[29] This is in contrast to Drossel and Kardar's update rule [17] where only particles at a site affected by the surface evolution are moved.
[30] P. M. Binder, M. Paczuski, and M. Barma, Phys. Rev. E **49**, 1174 (1994).
[31] B. Derrida, S. A. Janowsky, J. L. Lebowitz, and E. R. Speer, J. Stat. Phys. **73**, 813 (1993).
[32] A. L. Barabasi and H. E. Stanley, *Fractal Concepts in Surface Growth* (Cambridge University Press, Cambridge, 1995).
[33] I. S. Gradshteyn and I. M. Ryzhik, *Table of Integrals, Series, and Products* (Academic Press, Florida, 2000), Identity 6.576.4, 676.
[34] I. S. Gradshteyn and I. M. Ryzhik, *Table of Integrals, Series, and Products* (Academic Press, Florida, 2000), Identity 6.621.3, 692.
[35] P. Meakin, *Fractals, Scaling and Growth far from Equilibrium* (Cambridge University Press, Cambridge, 1998).